Title: From primordial clocks to circadian oscillators

Authors: Warintra Pitsawong[1,#,†], Ricardo A. P. Pádua[1,#], Timothy Grant[2,#,‡], Marc Hoemberger[1,$], Renee Otten[1,$], Niels Bradshaw[3], Nikolaus Grigorieff[2,§], Dorothee Kern[1,*]

Affiliations:

[1] Howard Hughes Medical Institute and Department of Biochemistry, Brandeis University, 415 South Street, Waltham, MA 02454, USA
[2] Janelia Research Campus, Howard Hughes Medical Institute, 19700 Helix Dr, Ashburn, VA 20147, USA
[3] Department of Biochemistry, Brandeis University, 415 South Street, Waltham, MA 02454, USA

[†] Present address: Biomolecular Discovery, Relay Therapeutics, Cambridge, MA 02139, USA
[‡] Present address: John and Jeanne Rowe Center for Research in Virology, Morgridge Institute for Research, Madison, 330 N Orchard Street, Madison, WI 53715, USA and Department of Biochemistry, University of Wisconsin-Madison, 433 Babcock Drive, Madison, WI 53706, USA
[$] Present address: Treeline Biosciences, 500 Arsenal Street, 2nd Floor, Watertown, MA 02472, USA
[§] Present address: Howard Hughes Medical Institute, RNA Therapeutics Institute, University of Massachusetts Chan Medical School, 368 Plantation Street, Worcester, MA 01605, USA

[#] these authors contributed equally to this work

[*] Correspondence and requests for materials should be addressed to D.K. (dkern@brandeis.edu)

Abstract:

Circadian rhythms play an essential role in many biological processes and surprisingly only three prokaryotic proteins are required to constitute a true post-translational circadian oscillator. The evolutionary history of the three Kai proteins indicates that KaiC is the oldest member and central component of the clock, with subsequent additions of KaiB and KaiA to regulate its phosphorylation state for time synchronization. The canonical KaiABC system in cyanobacteria is well understood, but little is known about more ancient systems that possess just KaiBC, except for reports that they might exhibit a basic, hourglass-like timekeeping mechanism. Here, we investigate the primordial circadian clock in *Rhodobacter sphaeroides* (RS) that contains only

KaiBC to elucidate its inner workings despite the missing KaiA. Using a combination X-ray crystallography and cryo-EM we find a novel dodecameric fold for $KaiC_{RS}$ where two hexamers are held together by a coiled-coil bundle of 12 helices. This interaction is formed by the C-terminal extension of $KaiC_{RS}$ and serves as an ancient regulatory moiety later superseded by KaiA. A coiled-coil register shift between daytime- and nighttime-conformations is connected to the phosphorylation sites through a long-range allosteric network that spans over 160 Å. Our kinetic data identify the difference in ATP-to-ADP ratio between day and night as the environmental cue that drives the clock and further unravels mechanistic details that shed light on the evolution of self-sustained oscillators.

Main Text:

Circadian clocks are self-sustained biological oscillators that are found ubiquitously in prokaryotic and eukaryotic organisms. In eukaryotes these systems are complex and very sophisticated, whereas in prokaryotes the core mechanism is regulated by a posttranslational oscillator that can be reconstituted *in vitro* with three proteins (*kaiA*, *kaiB*, and *kaiC*)[1] and ATP. Seminal work on the KaiABC system resulted in a comprehensive understanding of its circadian clock: KaiC is the central component that auto-phosphorylates through binding of KaiA and auto-dephosphorylates upon association with KaiB[2-5]. The interplay between these three proteins has been shown *in vitro* to constitute a true circadian oscillator characterized by persistence, resetting, and temperature compensation. Consequently, the KaiABC system is considered an elegant and the simplest implementation of a circadian rhythm. The evolutionary history of *kai* genes established *kaiC* as the oldest member dating back ~3.5 bya, with subsequent additions of *kaiB* and most recently *kaiA* to form the extant *kaiBC* and *kaiABC* clusters, respectively[6,7]. Interestingly, a few studies of more

primitive organisms that lack *kaiA* hinted that the *kaiBC*-based systems might provide already a basic, hourglass-like timekeeping mechanism[8-10]. Contrary to the self-sustained oscillators found in cyanobacteria, such a timer requires an environmental cue to drive the clock and for the daily "flip" of the hourglass. The central role of circadian rhythms in many biological processes, controlled by the day and night cycle on earth, makes their evolution a fascinating topic.

Here, we investigate such a primitive circadian clock by biochemical and structural studies of the KaiBC system of the purple, non-sulfur photosynthetic proteobacterium *Rhodobacter sphaeroides* KD131 (RS; hereafter referred to as $KaiB_{RS}$ and $KaiC_{RS}$). Surprisingly, the organism shows sustained rhythms of gene expression *in vivo*, but whether *kaiBC* is responsible for this observation remains inconclusive in the absence of a *kaiC* knockout[11]. A more recent study of the closely-related *Rhodopseudomonas palustris* demonstrated causality between the proto-circadian rhythm of nitrogen fixation and expression of the *kaiC* gene using a KO strain[10]. We discover using *in vitro* experiments that $KaiBC_{RS}$ is indeed a primordial circadian clock with a mechanism that is different from the widely studied circadian oscillator in *Synechococcus elongatus* PCC 7942 (hereafter referred to as $KaiABC_{SE}$)[2-5]. We identify an environmental cue that regulates the phosphorylation state and consequently produces a 24-hour clock *in vivo* as the switch in ATP-to-ADP ratio between day and night. Our kinetic results combined with X-ray and cryo-EM structures of the relevant states unravel a long-range allosteric pathway that is crucial for function of the hourglass and sheds light on the evolution of self-sustained oscillators. Notably, we find a novel protein fold for $KaiC_{RS}$ and uncover a register shift in the coiled-coil domain spanning ~115 Å as the key regulator in this system, which shows intriguing structural similarities to dynein signaling[12].

C-terminal tail as a primitive regulatory moiety

To gain insight into the evolution of the *kaiBC* cluster, we constructed a phylogenetic tree of *kaiC* after the emergence of the *kaiB* gene (Fig. 1a, Extended Data Fig. 1a). The first obvious question is how $KaiC_{RS}$ and other members in the clade can auto-phosphorylate despite having no KaiA, which is known to be crucial for this function in the canonical KaiABC system at its optimum temperature. We observe a large clade that exhibits a C-terminal tail about 50 amino acids longer compared to *kaiC* in other clades (Extended Data Fig. 1b). This C-terminal extension near the A-loop is predominantly found in the *kaiC2* subgroup, which was previously annotated as having two serine phosphorylation sites instead of the Thr/Ser pair found in *kaiC1* and *kaiC3* subgroups (Extended Data Fig. 1b)[13-15]. In *Synechococcus elongatus*, the binding of $KaiA_{SE}$ to the A-loop of $KaiC_{SE}$ tethers them in an exposed conformation[16] that activates both auto-phosphorylation and nucleotide exchange[17]. Given the proximity of the extended C-terminal tail to the A-loop we conjectured that it could serve as the "primitive" regulatory moiety made redundant concomitantly with the appearance of KaiA.

To test our hypothesis, we first measured the auto-phosphorylation and nucleotide exchange rates in $KaiC_{RS}$ that both depend heavily on the presence of KaiA in the $KaiABC_{SE}$ system. We observe an auto-phosphorylation rate for $KaiC_{RS}$ that is ~16-fold higher than for $KaiC_{SE}$ activated by $KaiA_{SE}$ ($6.5 \pm 1.0\ h^{-1}$ versus $0.40 \pm 0.02\ h^{-1}$, respectively; Fig. 1b and Extended Data Figs. 2a-e). Similarly, the nucleotide exchange is faster in $KaiC_{RS}$ compared to $KaiC_{SE}$ even in the presence of $KaiA_{SE}$ ($18.0 \pm 1.5\ h^{-1}$ compared to $4.7 \pm 0.3\ h^{-1}$, respectively; Fig. 1c and Extended Data Fig. 2f). Our data clearly show that $KaiC_{RS}$ can perform both auto-phosphorylation and nucleotide exchange on its own and, in fact, does so faster than its more recently evolved counterparts.

Coiled-coil interaction assembles KaiC$_{RS}$ dodecamer

To assess mechanistically how KaiC in the *kaiA*-lacking systems accomplishes auto-phosphorylation we turned to structural biology. The crystal structure of KaiC$_{RS}$, unlike KaiC from cyanobacteria, reveals a homododecamer consisting of two homohexameric domains joined by a twelve-helical coiled-coil domain that is formed by the extended C-terminal tail (PDB 8dba; Fig. 1d and Extended Data Table 1). A closer inspection of the CII domains in KaiC$_{RS}$ and KaiC$_{SE/TE}$ showed an obvious difference in A-loop orientations: an extended conformation in KaiC$_{RS}$ versus a buried orientation in KaiC$_{SE/TE}$ (Fig. 1e). The existence of such an extended conformation upon binding of KaiA was conjectured earlier based on the perceived hyper- and hypo-phosphorylation upon removing the A-loop or disrupting KaiA binding, respectively[18]. Importantly, a recent cryo-EM structure of the nighttime phosphomimetic KaiC$_{SE}$ S431E/T432A in its compressed state was solved and directly showed a disordered A-loop that no longer interacts with the 422-loop[19], similar to the extended A-loop conformation we observe in KaiC$_{RS}$ (Fig. 1e). The loss of interaction between the A-loop and 422-loop (just 10 residues apart from the phosphorylation sites), results in closer proximity between the hydroxyl group of Ser^{431}/Thr^{432} and the γ-phosphate of ATP, thereby, facilitating the phosphoryl-transfer step[20]. Furthermore, the sequence similarity between KaiC$_{RS}$ and KaiC$_{SE}$ is less than 30% for the A-loop and residues considered important for stabilization of this loop in its buried orientation (i.e., 422-loop and residues 438-444; Fig. 1e). Taken together, our structural and kinetic data support the idea that an exposed A-loop is key for KaiA-independent enhancement of nucleotide exchange and hence auto-phosphorylation in KaiC$_{RS}$ and perhaps other KaiBC-based systems.

Is the purpose of the coiled-coil domain merely to "pull up" the A-loop or does it actively participate in nucleotide exchange and auto-phosphorylation of KaiC? To further understand its

role, we generated a truncation at residue Glu^{490} based on the phylogenetic tree and crystallographic information ($KaiC_{RS}$-Δcoil; Extended Data Fig. 1b) to disrupt the coiled-coil interaction between the two hexamers. Indeed, the crystal structure of $KaiC_{RS}$-Δcoil (PDB 8db3; Fig. 2a,b and Extended Data Table 1) and its size-exclusion chromatogram and analytical ultracentrifugation profile (Extended Data Fig. 3a-c) show a hexameric structure with no coiled-coil interaction. Nucleotide exchange rates in the CII domain for $KaiC_{RS}$-Δcoil and wild type are comparable (19.1 ± 0.8 h^{-1} and 18.0 ± 1.5 h^{-1}, respectively; Extended Data Fig. 3d) as are the phosphorylation rates (5.5 ± 0.4 h^{-1} and 7.4 ± 0.3 h^{-1} for $KaiC_{RS}$-Δcoil and wild type, respectively; Extended Data Fig. 3e,f). These results indicate that the extended A-loop and not the coiled-coil interaction plays a pivotal role in nucleotide exchange and auto-phosphorylation in $KaiC_{RS}$, potentially explaining auto-phosphorylation in other KaiBC-based systems lacking a coiled-coil bundle. Notably, the coiled-coil bundle provides additional hexameric stability: the $KaiC_{RS}$ dodecamer is stable for extended periods of time in the presence of only ADP (Extended Data Fig. 3g,h), whereas for $KaiC_{SE}$ oligomers are not observed under these conditions[21].

Long-range allosteric network in $KaiC_{RS}$

The change in phosphorylation state of KaiC has been well established to be the central feature for the circadian rhythm[22,23]. Interestingly, when comparing the unphosphorylated form of full-length $KaiC_{RS}$ (PDB 8dba) and its phosphomimetic mutant (S413E/S414E, PDB xxxx, Extended Data Fig. 4, and Extended Data Table 2) we observe two distinct coiled-coil interactions. Upon phosphorylation, the coiled-coil pairs swap partners by interacting with the other neighboring chain from the opposite hexamer resulting in a register shift that propagates ~115 Å along the

entire coiled-coil (Fig. 2c and Extended Data Fig. 5). In the phosphomimetic state, the register comprises bulkier hydrophobic residues thus resulting in a more stable interaction than for the dephosphorylated form (Fig. 2d and Extended Data Fig. 3g). Furthermore, the C-terminal residues of $KaiC_{RS}$-S413E/S414E interact with the CII domain of the opposite hexamer, whereas the lack of electron density for the last 30 residues in the wild-type structure indicates more flexibility in the dephosphorylated state. Importantly, we discover that these conformational changes in the coiled-coil domain seem to be coupled through a long-range allosteric network to the phosphorylation sites. The rotameric states of residues Ser^{413}, Ser^{414}, Trp^{419}, Val^{421}, Tyr^{436}, Leu^{438}, Val^{449}, and Arg^{450} move concertedly and point towards the nucleotide-binding site when the protein is phosphorylated or away in the absence of a phosphate group (Fig. 2e, Extended Data Fig. 5d). We hypothesize that the proximity of the nucleotide to the phosphorylated residue allows for a more efficient phosphoryl transfer and, therefore, determined experimentally the impact of the coiled-coil domain on the auto-dephosphorylation of $KaiC_{RS}$. Indeed, we observe a noticeable effect: wild-type protein dephosphorylates comparatively quickly (k_{obs} = 11.5 ± 0.8 h^{-1}) in the presence of only ADP, whereas little dephosphorylation was observed for $KaiC_{RS}$-Δcoil (Fig. 2f and Extended Data Fig. 3i) where the allosteric propagation is disrupted (Extended Data Fig. 5d). Consistent with this accelerated dephosphorylation due to the coiled-coil domain, our crystallographic data show a phosphate-group on Ser^{414} for $KaiC_{RS}$-Δcoil but not for the wild-type protein (Fig. 2a and Extended Data Fig. 5d).

ATP-to-ADP ratio to reset the clock

The surprising result here is that $KaiC_{RS}$ can auto-dephosphorylate on its own despite being constitutively active for phosphorylation due to its extended A-loop conformation. In the canonical *kaiABC* system, the interaction between KaiB and KaiC is required to provide a new binding interface which sequesters KaiA from its "activating" binding site, thereby promoting auto-dephosphorylation at the organism's optimum temperature[24-26]. The obvious next questions are whether the $KaiC_{RS}$ system can oscillate and secondly if there is a regulatory role for $KaiB_{RS}$ in this process. Comparing the *in vitro* phosphorylation states of $KaiC_{RS}$ in the absence and presence of $KaiB_{RS}$ shows an initial, fast phosphorylation followed by an oscillatory-like pattern in the presence of $KaiB_{RS}$ (hereafter referred to as $KaiBC_{RS}$), whereas $KaiC_{RS}$ alone remains phosphorylated (Fig. 3a,b). Interestingly, the ATP consumption during the reaction with $KaiB_{RS}$ is significantly higher than without (Fig. 3a) and we have seen earlier that $KaiC_{RS}$ will dephosphorylate completely in the presence of only ADP (*cf.* Fig. 2f). These results suggest that the phosphorylation state of $KaiC_{RS}$ and thus the observed oscillatory half-cycle (Fig. 3a,b), is likely related to a change in ATP-to-ADP ratio and we conjectured this could constitute the environmental cue to reset the timer. To test our hypothesis, an ATP-recycling system was added after complete dephosphorylation of $KaiBC_{RS}$ and, as predicted, $KaiC_{RS}$ was able to restart the cycle and phosphorylate again (Extended Data Fig. 6a). Naturally, *in vivo* the ATP-to-ADP ratio will not vary as drastically as in this *in vitro* experiment since nucleotide homeostasis is tightly regulated. To mimic the day- and night-period for *Rhodobacter sphaeroides* we repeated the experiments while keeping the ATP-to-ADP ratio constant (mostly ATP at daytime due to photosynthesis versus 25:75% ATP:ADP during nighttime, respectively)[27]. In the presence of high ATP (i.e., mimicking daytime) $KaiC_{RS}$ remains singly or doubly phosphorylated (Fig. 3c and

Extended Data Fig. 6b) irrespective of $KaiB_{RS}$, whereas a constant 25:75% ATP-to-ADP ratio (i.e., mimicking nighttime) results in a much higher fraction of dephosphorylated $KaiC_{RS}$ in the presence of $KaiB_{RS}$ (Fig. 3c). Moreover, when the ATP-to-ADP ratio is flipped to mimic the daytime, $KaiC_{RS}$ is able to phosphorylate again (*cf*. Fig. 3c; around the 28-hour mark). Our data support the notion that the phosphorylation behavior depends strongly on the ATP-to-ADP ratio and, more importantly, demonstrate that the physical binding of $KaiB_{RS}$ results in a higher level of $KaiC_{RS}$ dephosphorylation at nighttime.

Next, we investigated the accelerated ATPase activity in $KaiC_{RS}$ upon complex formation. The ATPase activity reported for $KaiC_{SE}$ is very low (~15 ATP molecules day^{-1} $molecule^{-1}$ $KaiC_{SE}$) and was proposed as a reason for the "slowness"[28]. $KaiC_{RS}$ alone already shows a significantly faster ATPase rate that gets further enhanced by binding of $KaiB_{RS}$ (208 ± 19 and 1,557 ± 172 ATP molecules day^{-1} $KaiC_{RS}^{-1}$, respectively; left two bars in Fig. 3d and Extended Data Fig. 6c-g). Furthermore, $KaiC_{RS}$ exhibits no temperature compensation for its ATPase activity (Q_{10} ~1.9; Extended Data Fig. 6c), a feature that is present in $KaiC_{SE}$ and proposed to be a prerequisite for self-sustained rhythms[28]. The deviation from unity for Q_{10} is consistent with our earlier observation that the $KaiBC_{RS}$ system is not a true circadian oscillator but rather an hourglass-timer (*cf*. Fig. 3b).

Regulatory role of $KaiB_{RS}$

The mechanistic details of how KaiB binding in the CI domain allosterically affects the auto-dephosphorylation of $KaiC_{RS}$ in the CII domain remain unclear. Intuitively, there are three plausible scenarios to explain this, namely that $KaiB_{RS}$ binding (i) stimulates the phosphoryl-

transfer from pSer back to ADP (Extended Data Fig. 7a), (ii) increases the hydrolysis rate of the active-site ATP (Extended Data Fig. 8a), or (iii) accelerates the nucleotide exchange in the CII domain (Extended Data Fig. 8e). To differentiate between these possibilities, we performed radioactivity experiments to follow nucleotide interconversion, measured ATPase activity for wild-type $KaiC_{RS}$ and mutant forms that are incapable of ATPase activity in the CI or CII domain, and quantified nucleotide-exchange rates by fluorescence using mant-ATP. First, we detected fast, transient ^{32}P-ATP formation in our radioactivity experiments when starting from ^{32}P-phosphorylated $KaiC_{RS}$ due to its ATP-synthase activity in the CII domain (Fig. 3e and Extended Data Fig. 7b-d). The observed phosphoryl-transfer rate is independent of $KaiB_{RS}$ (k_{obs} = 12.0 ± 1.7 h^{-1} and 15.4 ± 1.7 h^{-1} in its absence and presence, respectively; Fig. 3f) and agrees well with the rates determined from our gel electrophoresis experiments (11.0 ± 0.8 h^{-1} and 11.5 ± 0.8 h^{-1} with/without $KaiB_{RS}$, respectively; Extended Data Fig. 7e,f). Our experimental data confirm that $KaiC_{RS}$ undergoes dephosphorylation via an ATP-synthase mechanism similarly to what was observed for $KaiC_{SE}$[29]; KaiB does not expedite the actual phosphoryl-transfer reaction, which is never the rate-limiting step. Since we were unable to stabilize the first phosphorylation site (Ser^{414}) in the presence of ADP, the rates reported here correspond exclusively to dephosphorylation of Ser^{413}. Secondly, to deconvolute the contributions of the CI and CII domains to the observed ATPase activity, we measured ADP production by $KaiC_{RS}$ mutants that abolish hydrolysis in either the CI ($KaiC_{RS}$-E62Q/E63Q) or CII ($KaiC_{RS}$-E302Q/E303Q) domain. For wild-type $KaiC_{RS}$, the binding of $KaiB_{RS}$ results in a 7.5-fold increase in ATPase activity, and we show that both domains are affected and contribute additively (3-fold for CI and at least 1.7-fold for CII, respectively) to the overall effect (Fig. 3d and Extended Data Fig. 8b-d). Of note, the fold increase in the CII domain represents a lower limit since the $KaiC_{RS}$-E62Q/E63Q mutations interfere with $KaiB_{RS}$

binding as reported before for $KaiC_{SE}$[30]. Thirdly, our measurements of the nucleotide exchange rate show that it is also unaffected by $KaiB_{RS}$ binding ($19.8 \pm 1.8\ h^{-1}$ and $18.0 \pm 1.5\ h^{-1}$ with/without, respectively; Fig. 3g); since there is no Trp residue near the nucleotide binding site in the CI domain, only the exchange rate in the CII domain could be determined. Interestingly, the change in fluorescence amplitude is much smaller in the presence of $KaiB_{RS}$, demonstrating that even though the binding of $KaiB_{RS}$ does not accelerate nucleotide exchange, it appears to induce a conformational rearrangement in the CII domain especially at higher temperature (Fig. 3g and Extended Data Fig. 8f-h).

Structure of KaiBC$_{RS}$ complex

To elucidate the structural underpinning of the faster ATPase activity upon $KaiB_{RS}$ binding, we solved the cryo-EM structures of $KaiC_{RS}$ alone (PDB xxxx) and in complex with $KaiB_{RS}$ (PDB xxxx) (Extended Data Table 2). Twelve $KaiB_{RS}$ molecules (monomeric in solution, Extended Data Fig. 9a) bind to the CI domain of the $KaiC_{RS}$-S413E/S414E dodecamer (Fig. 4a-c and Extended Data Fig. 9b). The bound state of $KaiB_{RS}$ adopts the same "fold-switch" conformation as observed for $KaiB_{TE}$[25] and suggests that this is the canonical binding-competent state (Fig. 4b). Upon binding of $KaiB_{RS}$, the CI-CI interfaces loosen up (Fig. 4c), which allows for the formation of a tunnel that connects bulk solvent to the position of the hydrolytic water in the active sites (Fig. 4d and Extended Data Fig. 9c). There are other lines of evidence for the weakened interactions within the CI domains. First, $KaiB_{RS}$ binding to either $KaiC_{RS}$-CI domain (Extended Data Fig. 10a) or $KaiC_{RS}$-Δcoil (i.e., missing the C-terminal extensions; Extended Data Fig. 10b) results in disassembly of the hexameric $KaiC_{RS}$ structure into its monomers. In contrast, full-length $KaiC_{RS}$ maintains its oligomeric state upon binding of $KaiB_{RS}$ likely due to the stabilization provided by

the coiled-coil interaction. Secondly, a decrease in melting temperature (T_M) of $KaiC_{RS}$ is observed with increasing $KaiB_{RS}$ concentration (Extended Data Fig. 10c). There is no interaction between neighboring $KaiB_{RS}$ molecules within the complex (Extended Data Fig. 9b), suggesting a non-cooperative assembly of $KaiB_{RS}$ to $KaiC_{RS}$ contrary to what is observed for the $KaiBC_{SE/TE}$ complex[31,32].

Furthermore, we noticed that KaiB-bound structures in phosphomimetic variants of $KaiC_{RS}$ (Fig. 4c,d) and $KaiC_{SE}$[26] have ADP bound in their CI domain, demonstrating that the post-hydrolysis state is also the binding-competent state for $KaiB_{RS}$. To test this hypothesis, a His-tagged $KaiB_{RS}$ protein was used in pull-down assays to detect its physical interaction with wild-type and mutant forms of $KaiC_{RS}$ bound with either ADP or ATP. Nearly all $KaiB_{RS}$ is complexed to ADP-bound $KaiC_{RS}$, whereas less than 30% co-elutes in the ATP-bound form regardless of the phosphorylation state (Fig. 4e and Extended Data Fig. 10d,e). The complex formation depends inversely on the ATP-to-ADP ratio (Extended Data Fig. 10f). We performed fluorescence anisotropy competition experiments for a more quantitative description of the binding interaction between $KaiC_{RS}$ and $KaiB_{RS}$: very similar K_D values were obtained for unphosphorylated, wild-type $KaiC_{RS}$ (Fig. 4f) and its phosphomimetic form (Extended Data Fig. 10g) bound with ADP (0.42 ± 0.03 μM and 0.79 ± 0.06 μM, respectively). No measurable binding curves were obtained for ATP-bound phosphorylated wild-type $KaiC_{RS}$ (Fig. 4f) or $KaiC_{RS}$-S413E/S414E (Extended Data Fig. 10g) with ATP-recycling system, likely due to the small fraction of complex present. Our data show that the post-hydrolysis state in the CI domain is key for $KaiB_{RS}$ binding, whereas the phosphorylation state of $KaiC_{RS}$ has only a marginal effect.

In summary, we unequivocally demonstrate that binding of $KaiB_{RS}$ at the CI domain in the post-hydrolysis state facilitates the hydrolysis of transiently formed ATP after dephosphorylation

of $KaiC_{RS}$ in the CII domain (Fig. 4g). Our fluorescence experiments (Fig. 3g and Extended Data Fig. 8f) detect a conformational change in the CII domain upon $KaiB_{RS}$ binding, but we do not observe major structural changes in the cryo-EM structures. Based on the temperature dependence of the fluorescence amplitudes (Extended Data Fig. 8f) we conjecture that the inability to detect conformational differences is likely because of the low temperature. Since the CII domain prefers to bind ATP over ADP (Extended Data Fig. 10h), ATP hydrolysis in the CII domain stimulated by $KaiB_{RS}$ is particularly important to keep $KaiC_{RS}$ in its dephosphorylated state at nighttime, where the exogenous ATP-to-ADP ratio remains sufficiently high to otherwise result in ATP-binding in the CII active site (*cf.* Fig. 3c and Extended Data Fig. 6b).

Discussion

The $KaiBC_{RS}$ system studied here represents a primordial, hourglass timekeeping machinery and its mechanism provides insight into more evolved circadian oscillators like KaiABC. The dodecameric $KaiC_{RS}$ shows constitutive kinase-activity due to its extended C-terminal tail that forms a coiled-coil bundle with the opposing hexamer and elicits a conformation akin to the exposed A-loop conformation in $KaiAC_{SE}$, and auto-phosphorylation occurs within half an hour. In the $KaiABC_{SE}$ system, the transition from unphosphorylated to doubly phosphorylated KaiC takes place over about twelve hours and the fine-tuning of this first half of the circadian rhythm is accomplished by the emergence of $KaiA_{SE}$ during evolution. The second clock protein, KaiB, binds at the CI domain with the same "fold-switched" state in both systems. The interaction is controlled by the phosphorylation state in the $KaiABC_{SE}$ system, and its sole function is to sequester $KaiA_{SE}$ from the "activating" binding site, whereas KaiB binding directly accelerates the ATPase activity in the $KaiBC_{RS}$ system regardless of the phosphorylation state. The $KaiBC_{RS}$

system requires an environmental switch in ATP-to-ADP concentration to reset the clock and thus follows the day-night schedule when nucleotide concentrations inherently fluctuate in the organism. By contrast, the self-sustained oscillator $KaiABC_{SE}$ remains functional over a wide range of nucleotide concentrations and responds to changes in the ATP-to-ADP ratio by changing its phosphorylation period and amplitude to remain entrained with the day and night cycle[33].

The novel structural fold of KaiC utilizes the versatile coiled-coil architecture as part of a long-range allosteric network that regulates $KaiC_{RS}$ dephosphorylation. Nature uses conformational changes in coiled-coil domains for a variety of regulatory functions[34], including the activity of the motor protein dynein in cellular transport of cargo along the actin filament[12]. A similar register shift, although in a coiled-coil interaction formed by only two helices is used in dynein motility. Given that this simple heptad repeat sequence emerged multiple times and is found throughout all kingdoms of life[35] it is an example of convergent evolution.

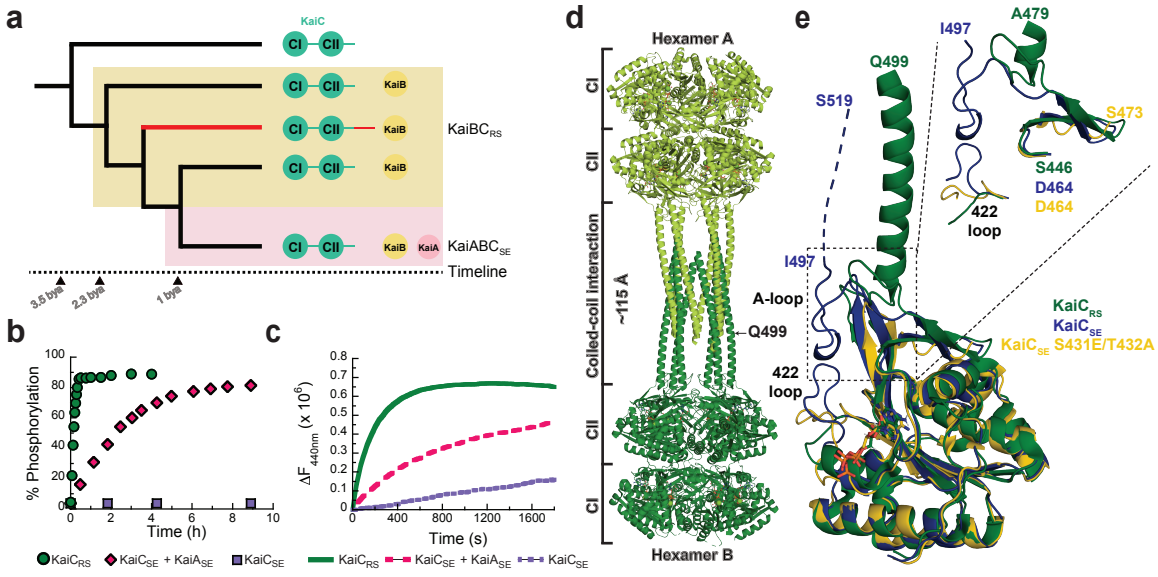

Fig. 1. Extended C-terminal tail of KaiC$_{RS}$ forms a coiled-coil interaction with an exposed A-loop for KaiA-independent phosphorylation of KaiC. (a) Schematic phylogenetic tree of *kaiC* showing the appearance of *kaiB* and *kaiA* during evolution. The *kaiC* clade with an approximately 50 amino acids C-terminal extension is labeled in red and a timeline was predicted as previously reported[6] **(b)** Phosphorylation over time of KaiC$_{RS}$ (green circles, 6.5 ± 1.0 h^{-1}) and KaiC$_{SE}$ in the presence (pink circles, 0.40 ± 0.02 h^{-1}) or absence (purple circles) of KaiA$_{SE}$ at 30 °C. The standard deviation in reported parameters are obtained from the fitting. **(c)** Nucleotide exchange between ATP and mant-ATP in KaiC$_{RS}$ alone (green trace, 18.0 ± 1.5 h^{-1}) compared to KaiC$_{SE}$ in the presence (pink trace, 4.7 ± 0.3 h^{-1}) and absence of KaiA$_{SE}$ (purple trace, 0.08 ± 0.04 h^{-1}) measured by fluorescence at 30 °C. Representative traces are shown and the fitted parameters (mean ± S.D) were obtained from three replicate measurements. **(d)** X-ray structure of dodecameric KaiC$_{RS}$ (PDB 8dba) colored by hexamer A (light green) and hexamer B (dark green). The CI, CII, and coiled-coil domains are indicated in (a), and the A-loop is labeled in (e). **(e)** Superposition based on alignment of the CII domain of KaiC$_{RS}$ (green, PDB 8dba, chain B), KaiC$_{SE}$ (purple, PDB 1tf7, chain B)[36], and KaiC$_{SE}$ S431E/T432A (yellow, PDB 7s65, chain A)[19] shows that KaiC$_{RS}$ has an extended A-loop orientation that no longer forms the inhibitory interaction with the 422-loop (KaiC$_{SE}$ numbering). The conformation of the 422-loop in KaiC$_{RS}$ resembles the one seen in the cryo-EM structure of the phosphomimetic KaiC$_{SE}$ S431E/T432A (yellow, PDB 7s65)[19]. No electron density is observed for the C-terminal part of wild-type KaiC$_{SE}$ and S431E/T432A mutant due to flexibility, and the missing 22 residues for wild-type KaiC$_{SE}$ (46 for S431E/T432A) are represented by a dashed line for wild-type KaiC$_{SE}$ (not shown for the mutant).

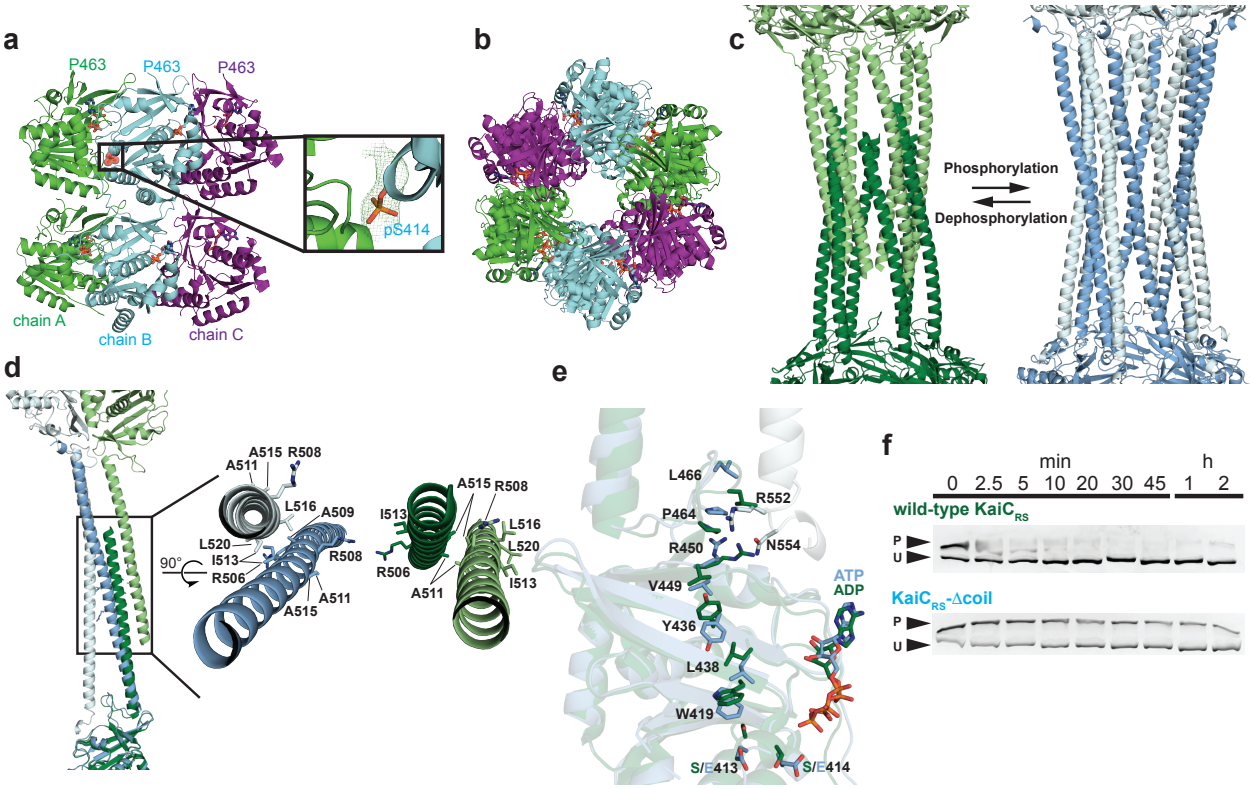

Fig. 2. Coiled-coil partner switch coupled to an allosteric network in the CII domain promotes auto-dephosphorylation. (a) The X-ray structure of KaiC$_{RS}$-Δcoil was solved in the C222$_1$ space group and contained three monomers in the asymmetric unit with ADP present in all active sites. The obtained electron density map allowed for model building up to Pro^{463}, indicating that the truncation at position 490 results in enhanced flexibility beyond Pro^{463}. Phosphorylation of Ser^{414} was observed in chain B (cyan) as shown by the electron density mFo-DFc polder map (green mesh, 3σ contour level). **(b)** Assembly analysis using the PISA software[37] revealed a hexamer as the most probable quaternary structure (top view). **(c)** Structural comparison of the coiled-coil domain for unphosphorylated KaiC$_{RS}$ (dark and light green; X-ray structure) and the KaiC$_{RS}$-S413E/S414E phosphomimetic mutant (dark and light blue; cryo-EM structure). (**d**) Overlay of interacting dimers of the structures in (c) using CII domain of chain A as reference (dark shades; bottom). Unphosphorylated KaiC$_{RS}$ (dark green) interacts with the opposite partner on the right (light green), whereas KaiC$_{RS}$-S413E/S414E (dark blue) interacts with the partner on the left (light blue). The hydrophobic packing in the coiled-coil domain is mediated by only the C$^{\beta}$ atoms of alanine and arginine residues in unphosphorylated KaiC$_{RS}$ but involves the entire side chain of leucine and isoleucine residues in the phosphomimetic structure. (**e**) Allosteric network in the phosphomimetic state (blue) from the coil (light blue) propagating through the KaiC$_{RS}$ CII domain to the active site (dark blue) compared to the unphosphorylated state (dark green)**. (f)** Auto-dephosphorylation of KaiC$_{RS}$ and KaiC$_{RS}$-Δcoil over time in the presence of 4 mM ADP at 30 °C. The phosphorylated (P) and unphosphorylated (U) proteins were separated by Zn^{2+} Phos-tag^{TM} SDS-PAGE.

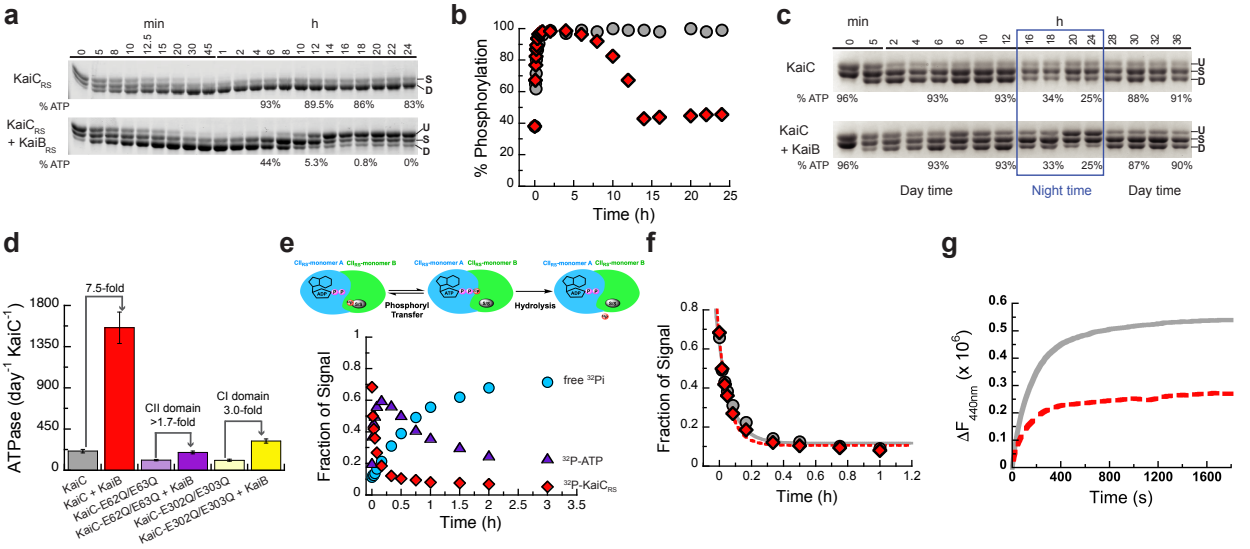

Fig. 3. The regulatory role of KaiB$_{RS}$ in the phosphorylation/dephosphorylation cycle of KaiC$_{RS}$. (a) SDS-PAGE gel of 3.5 μM KaiC$_{RS}$ and 4 mM ATP in the absence (upper gel) and presence (lower gel) of 3.5 μM KaiB$_{RS}$ at 35 °C with the percentage of ATP indicated at specific time points. U, S, and D represent unphosphorylated, singly, and doubly phosphorylated KaiC$_{RS}$, respectively. **(b)** Phosphorylation (single + double) of KaiC$_{RS}$ during the reaction in the absence (gray circles) or presence (red diamonds) of KaiB$_{RS}$ demonstrates its role in the dephosphorylation of KaiC$_{RS}$. **(c)** Phosphorylation-dephoshorylation cycle of 3.5 μM phosphorylated KaiC$_{RS}$ in the absence and presence of 3.5 μM KaiB$_{RS}$ in a constant ATP-to-ADP ratio of high ATP (4 mM) to mimic daytime and about 25% ATP to mimic the nighttime (exact percentage of ATP indicated at specific time points) at 30 °C. U, S, and D in both panels represent the unphosphorylated, singly phosphorylated (at Ser^{413} or Ser^{414}), and doubly phosphorylated state of KaiC$_{RS}$, respectively. These data show that the physical binding of KaiB$_{RS}$ is crucial to dephosphorylate KaiC$_{RS}$ at nighttime where ATP concentrations are still sufficiently high to otherwise keep KaiC$_{RS}$ in the phosphorylated state. **(d)** ATPase activity of wild-type KaiC$_{RS}$ in the absence (gray bar) and presence (red bar) of KaiB$_{RS}$, KaiC$_{RS}$-E62Q/E63Q in the absence (light purple bar) and presence (dark purple bar) of KaiB$_{RS}$, and KaiC$_{RS}$-E302Q/E303Q in the absence (light yellow bar) and presence (dark yellow bar) of KaiB$_{RS}$ at 30 °C. Bar graphs show mean ± S.D from three replicates. **(e)** Time-dependent auto-dephosphorylation of ^{32}P-labeled KaiC$_{RS}$ bound with ADP in the presence of 20 μM KaiB$_{RS}$ and 4 mM ADP at 30 °C showing phosphorylated ^{32}P-KaiC$_{RS}$ (red diamonds), ^{32}P-ATP (purple triangles), and free ^{32}Pi (cyan circles). The reaction products were separated by TLC. **(f)** The decay of phosphorylated ^{32}P-KaiC$_{RS}$ bound with 4 mM ADP in the absence (gray circles) and presence (red diamonds) of KaiB$_{RS}$ at 30 °C is obtained from autoradiography quantification (see Extended Data Fig. 7). **(g)** The nucleotide exchange of 3.5 μM KaiC$_{RS}$ (gray trace) and 3.5 μM KaiC$_{RS}$ in complex with 30 μM KaiB$_{RS}$ (red dotted trace) in the presence of ATP with mant-ATP. The proteins were incubated at 30 °C for 24 h before the addition of mant-ATP. Representative traces are shown and the fitted parameters (mean ± S.D) were obtained from three replicate measurements.

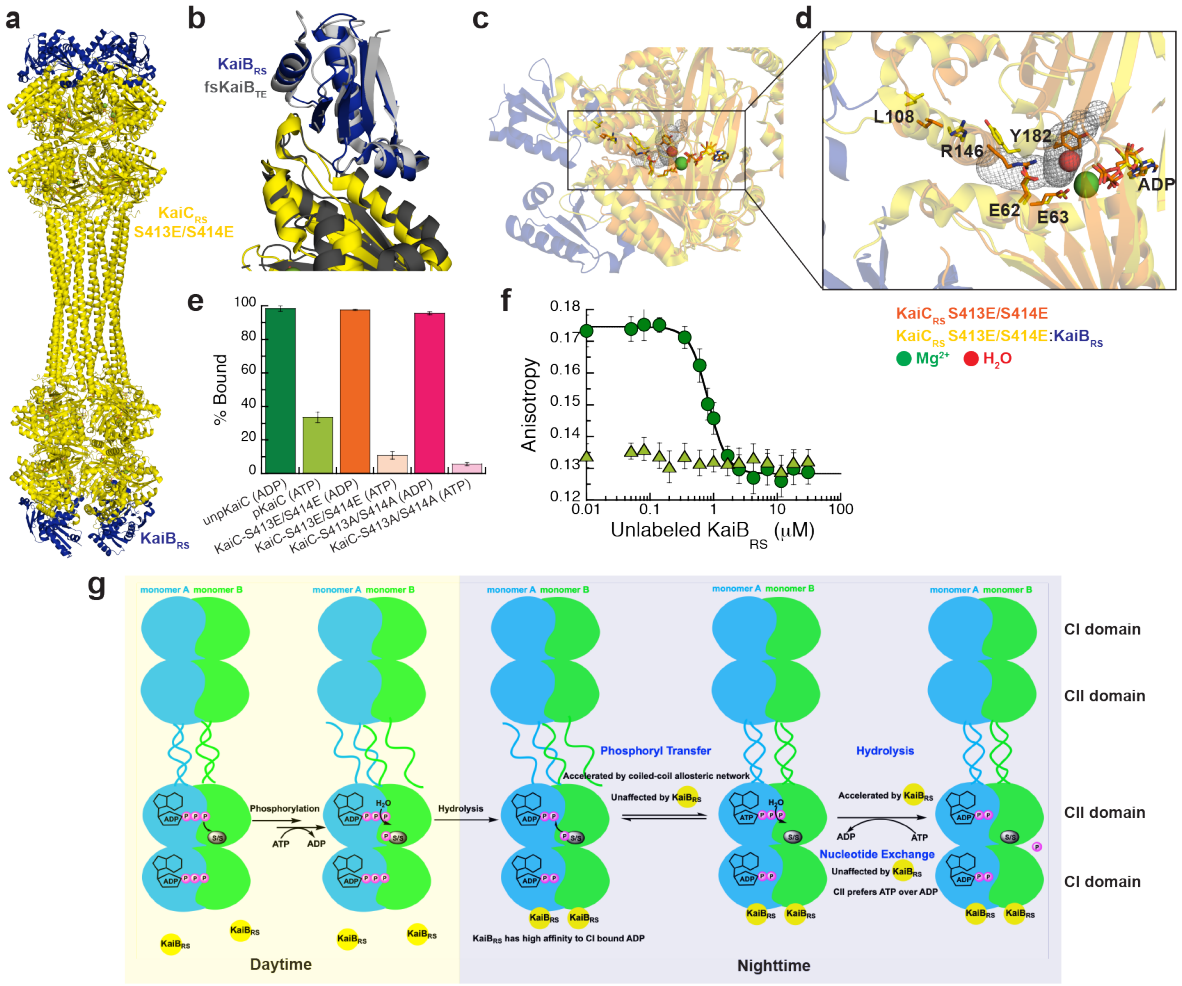

Fig. 4. KaiB$_{RS}$ binds to post-hydrolysis state and accelerates the ATPase activity of KaiC$_{RS}$. **(a)** Cryo-EM structure of KaiC$_{RS}$-S413E/S414E (yellow) in complex with KaiB$_{RS}$ (blue) (PDB xxxx). **(b)** Superposition of KaiC$_{RS}$-S413E/S414E (yellow) bound to KaiB$_{RS}$ (blue) (PDB xxxx) and KaiC$_{TE}$-S413E (dark gray) bound to fsKaiB$_{TE}$ (light gray) (PDB 5jwq[26]). **(c, d)** Binding of KaiB$_{RS}$ (blue) creates a tunnel (gray mesh) that enables water to reach the catalytic position (red sphere) for ATP hydrolysis in the CI domain. **(e)** Binding of wild-type and mutants forms of KaiC$_{RS}$ to His-tagged KaiB$_{RS}$ in the presence of ADP or ATP/recycling system at 25 °C. Bar graphs show mean ± S.D. from three replicates. **(f)** Fluorescence anisotropy of unlabeled KaiB$_{RS}$ competitively displacing KaiB$_{RS}$-6IAF (where 6IAF is the fluorophore) from unphosphorylated KaiC$_{RS}$ in the presence of ADP (dark green circles) and phosphorylated KaiC$_{RS}$ in the presence of the ATP/recycling system (light green triangles) at 30 °C. The average anisotropy and standard error were calculated from ten replicate measurements. **(g)** Schematic diagram of the uncovered mechanism of KaiC$_{RS}$ regulated by coiled-coil interaction and KaiB$_{RS}$ in the CI and CII domain.

Data availability: Structure factors and refined models are deposited in the Protein Data Bank (PDB) under accession codes 8dba (wild-type $KaiC_{RS}$, x-ray), 8db3 ($KaiC_{RS}$-Δcoil, x-ray), xxxx ($KaiC_{RS}$-S413E/S414E, cryo-EM), and xxxx ($KaiC_{RS}$-S413E/S414E:$KaiB_{RS}$, cryo-EM), respectively. Cryo-EM maps are deposited in the Electron Microscopy Data Bank (EMDB) under accession codes xxxx ($KaiC_{RS}$-S413E/S414E) and xxxx ($KaiC_{RS}$-S413E/S414E:$KaiB_{RS}$), respectively.

Acknowledgements:

D.K. and N.G. are supported by the Howard Hughes Medical Institute (HHMI). We would like to thank Mike Rigney for assistance with negative-stain data collection at the Brandeis University Electron Microscopy Facility, and Zhiheng Yu and the staff of the Janelia Research Campus cryo-EM facility for advice and assistance with data collection. The Berkeley Center for Structural Biology is supported in part by HHMI. Beamline 8.2.1 of the Advanced Light Source, a U.S. DOE Office of Science User Facility under Contract No. DE-AC02-05CH11231, is supported in part by the ALS-ENABLE program funded by the National Institutes of Health, National Institute of General Medical Sciences, grant P30 GM124169-01. Mass spectral data were obtained at the University of Massachusetts Mass Spectrometry Core Facility, RRID:SCR_019063.

Author contributions: W.P., R.A.P.P., and D.K. conceived the project and designed experiments. W.P. performed and analyzed all biochemical data. W.P. and R.A.P.P. set up the crystal trays and R.A.P.P. collected and analyzed the X-ray crystallographic data. W.P. prepared the samples for the cryo-EM studies and collected negative stain images to screen for optimal sample conditions;

T.G. collected and processed all cryo-EM data, and reconstructed the cryo-EM maps under supervision of N.G.; R.A.P.P. built and interpreted the structural models. W.P. and N.B. performed and analyzed experiments with radioactively labeled KaiC. M.H. built the KaiC phylogeny. W.P., R.O., and D.K. wrote the paper; and all authors commented on the manuscript and contributed to data interpretation.

Competing interests: D.K. is co-founder of Relay Therapeutics and MOMA Therapeutics. The remaining authors declare no competing interests.

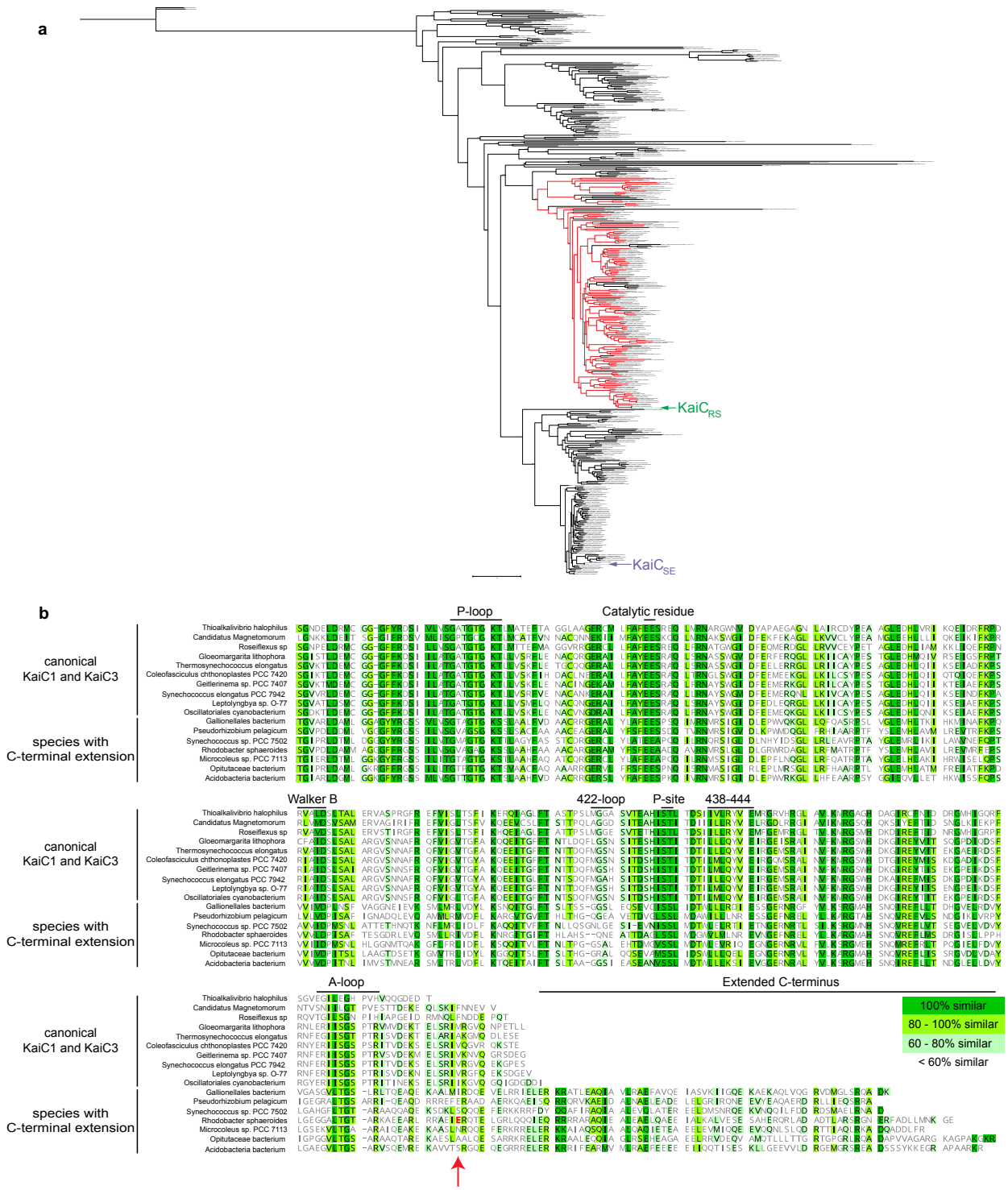

Extended Data Fig. 1 | Evolution of *kaiC* and sequence alignment of *kaiC* subgroups. (a) Phylogenetic tree of *kaiC* homologs, where *kaiC* genes that have an approximately 50 amino acids C-terminal extension are labeled in red. *Rhodobacter sphaeroides* strain KD131 studied here and *Synechococcus elongatus* PCC 7942 (widely studied in the literature) are highlighted in green and pink, respectively. The accession code and organism are shown at the tip of the branches, the numbers at each node represent the aBayes bootstrap values[38], and the legend for branch length is shown. **(b)** A sequence alignment of the CII domain of the *kaiC* subgroups annotated with its sequence similarity. Residue Glu^{490}, the position where the stop codon was introduced in the truncated KaiC$_{RS}$-Δcoil construct, is shown in red and marked with an arrow.

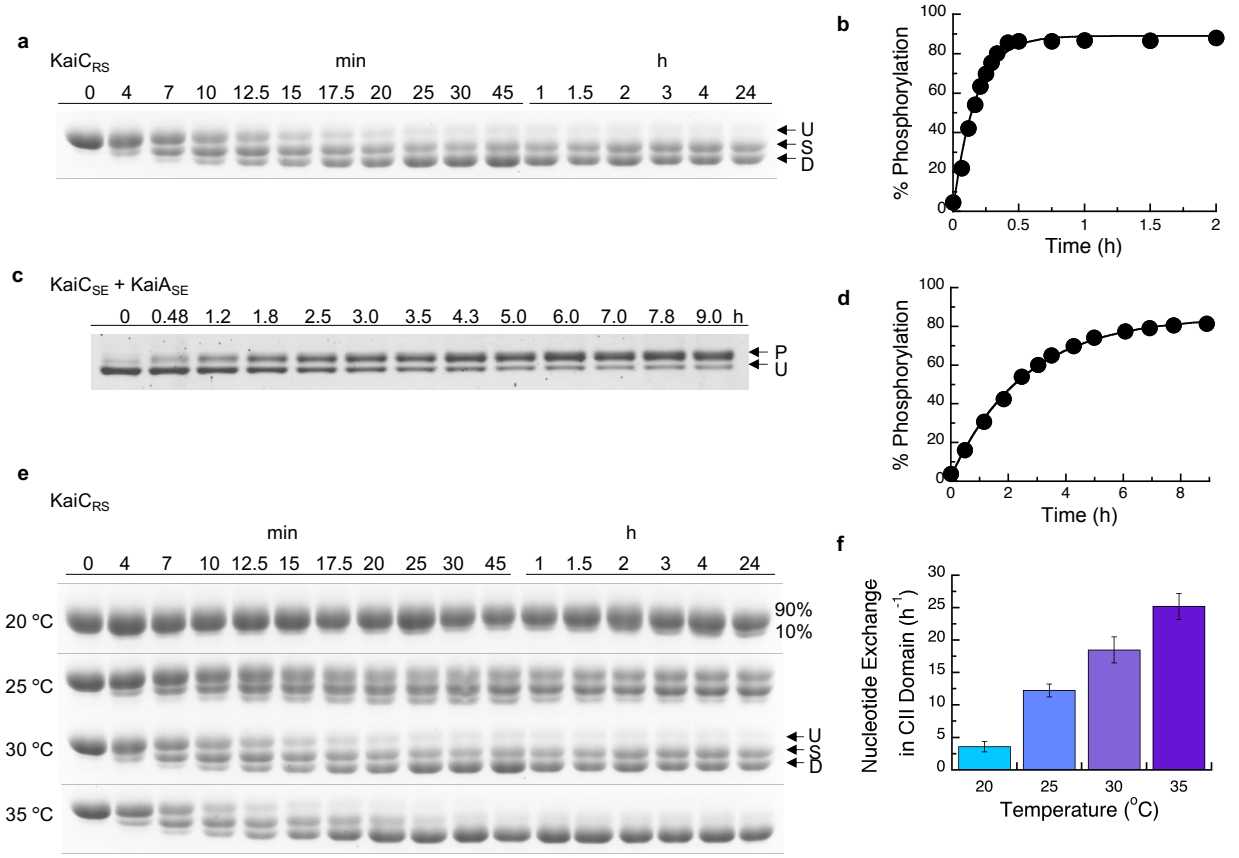

Extended Data Fig. 2 | Auto-phosphorylation and nucleotide exchange rates of KaiC. (a) 10% SDS-PAGE gel of 3.5 μM KaiC$_{RS}$ in the presence of 4 mM ATP and using an ATP-recycling system at 30 °C. U, S, and D represent unphosphorylated, singly, and doubly phosphorylated KaiC$_{RS}$, respectively. **(b)** Densitometric analysis of auto-phosphorylation (single + double phosphorylation) from panel (a) over time yields a rate of 6.5 ± 1.0 h^{-1}. **(c)** 6.5% SDS-PAGE gel of 3.5 μM KaiC$_{SE}$ in the presence of 1.2 μM KaiA$_{SE}$ and 4 mM ATP at 30 °C. U and P represent unphosphorylated and phosphorylated KaiC$_{SE}$, respectively. **(d)** Densitometric analysis of auto-phosphorylation of KaiC$_{SE}$ activated by KaiA$_{SE}$ (panel (c)) shows a rate of 0.40 ± 0.02 h^{-1} and is substantially slower than for KaiC$_{RS}$. The standard deviation for parameters in (b) and (d) were obtained from data fitting. **(e)** 10% SDS-PAGE gels for experiments with 3.5 μM KaiC$_{RS}$ in the presence of 4 mM ATP and using an ATP-recycling system between 20 and 35 °C show that the level of phosphorylation increases with temperature. U, S, and D represent unphosphorylated, singly, and doubly phosphorylated KaiC$_{RS}$, respectively. **(f)** Bar graphs indicating the nucleotide exchange rate in the CII domain of KaiC$_{RS}$ incubated with 50 μM ATP in the presence of an ATP-recycling system, and then mixed with 250 μM mant-ATP. An increase in fluorescence intensity at 440 nm was recorded and the single-exponential time traces were fitted to obtain the exchange rate constants: 3.6 ± 0.8 h^{-1} (20 °C), 12.2 ± 1.0 h^{-1} (25 °C), 18.5 ± 1.5 h^{-1} (30 °C), and 25.2 ± 0.2 h^{-1} (35 °C). Experiments were performed in triplicate with error bars representing SD.

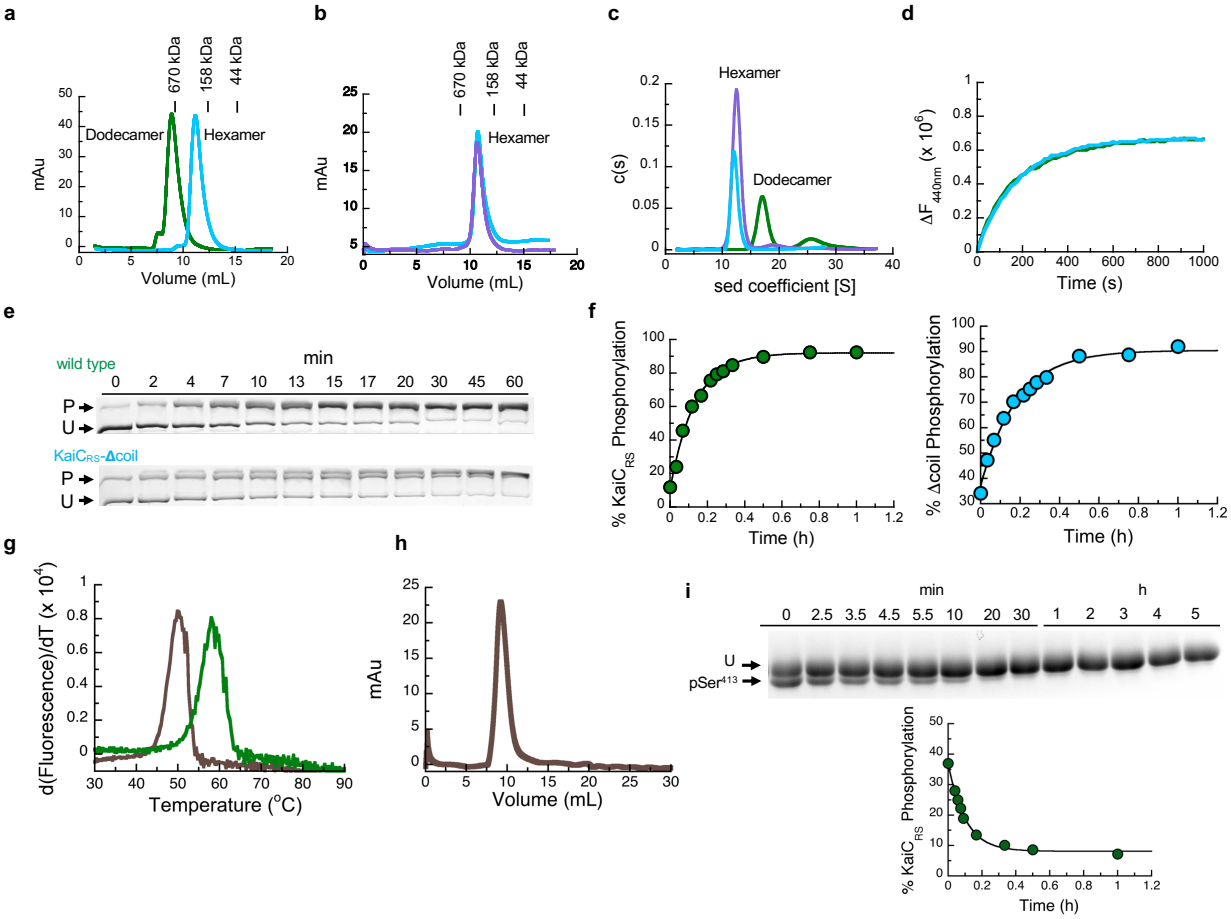

Extended Data Fig. 3 | Oligomeric states of KaiC$_{RS}$ and effect of coiled-coil domain on rates of nucleotide exchange and auto-phosphorylation. (a) Oligomerization analysis of KaiC$_{RS}$ (dodecamer, green line) and truncated KaiC$_{RS}$-Δcoil (hexamer, cyan line) by analytical gel-filtration chromatography. The protein size markers are indicated at the top. **(b)** Comparison of the elution profiles of KaiC$_{RS}$-Δcoil (cyan line) and KaiC$_{SE}$ (purple line) from size-exclusion chromatography shows a hexameric state for both KaiC$_{RS}$ Δcoil and KaiC$_{SE}$. **(c)** Oligomeric states of KaiC$_{RS}$ (dodecamer, green line), KaiC$_{RS}$-Δcoil (hexamer, cyan line), and KaiC$_{SE}$ (hexamer, purple line) were also measured by analytical ultracentrifugation (sedimentation velocity at 30,000 rpm and 20 °C) and the results agree with the data shown in panels (d) and (e). The graph in panel (f) represents the sedimentation coefficient distribution [c(s)]. **(d)** The change in fluorescence at 440 nm (ΔF_{440nm}) represents the nucleotide exchange between ATP and mant-ATP at 30 °C for KaiC$_{RS}$ (green trace, 18.0 ± 1.5 h^{-1}) and KaiC$_{RS}$-Δcoil (cyan trace, 19.1 ± 0.8 h^{-1}). Representative traces are shown and the fitted parameters (mean ± S.D) were obtained from three replicate measurements. **(e)** Zn^{2+} Phos-tag^{TM} SDS-PAGE gel shows the level of phosphorylation over time of KaiC$_{RS}$ (upper gel) and KaiC$_{RS}$-Δcoil (lower gel) at 35 °C. P and U represent phosphorylated and unphosphorylated protein, respectively. **(f)** Phosphorylation level over time of KaiC$_{RS}$ (green circles, 7.4 ± 0.3 h^{-1}) and KaiC$_{RS}$-Δcoil (cyan circles, 5.5 ± 0.4 h^{-1}) analyzed by densitometric analysis of Zn^{2+} Phos-tag^{TM} SDS-PAGE gel in (b). **(g)** First derivative of thermal-stability curves measured for unphosphorylated KaiC$_{RS}$ bound with ADP (brown line) and phosphorylated KaiC$_{RS}$ bound with ATP (green line). The extracted temperatures of denaturation are 50 °C (unphosphorylated KaiC$_{RS}$ in the presence of 1 mM ADP) and 58 °C (phosphorylated KaiC$_{RS}$ in the presence of 1 mM ATP), respectively. **(h)** Dodecameric state of unphosphorylated KaiC$_{RS}$ (40 μM) bound with ADP measured by size-exclusion chromatography. **(i)** SDS-PAGE gel shows dephosphorylation of Ser^{413} over time at 30 °C in the presence of 4 mM ADP (U and pSer^{413} represent unphosphorylated and Ser^{413}-phosphorylated KaiC$_{RS}$, respectively) with the corresponding kinetics shown in the lower panel (confirmed by MS/MS) with a rate constant of 11.5 ± 0.8 h^{-1}. This result suggests that the coiled-coil domain promotes KaiC$_{RS}$ dephosphorylation. The standard deviation for parameters in (f) and (i) were obtained from data fitting.

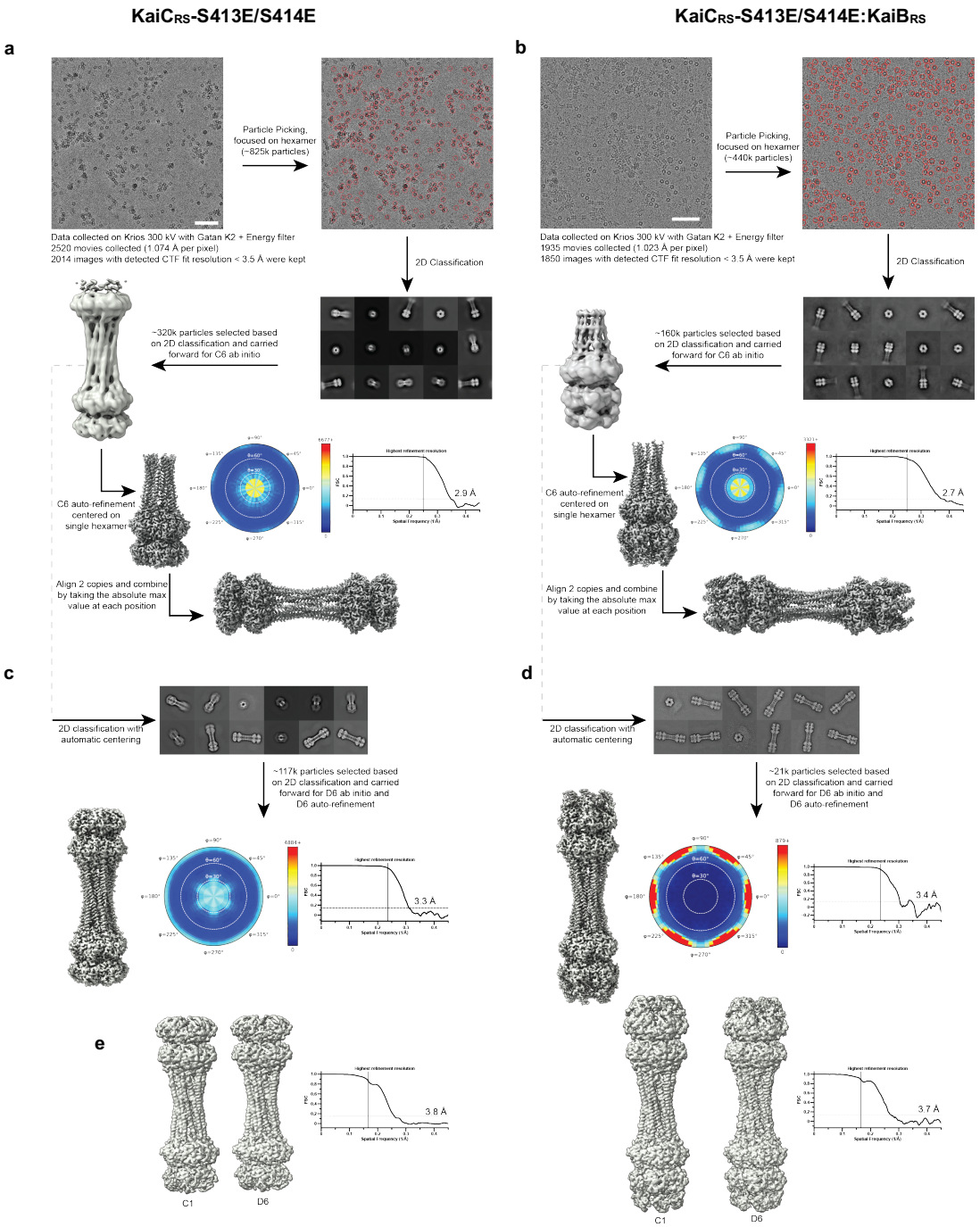

Extended Data Fig. 4 | Graphical description of the cryo-EM processing workflow and validation of the final dodecamer structures. The workflow (see description in Methods section) demonstrates a typical image (scale bar: 100 nm) and representative good class averages. The ab initio and final reconstructions are shown. Shown alongside the final reconstruction is the angular plot demonstrating the distribution of particle views and the Fourier shell correlation curve used for the global resolution estimation **(a)** KaiC$_{RS}$-S413E/S414E alone and **(b)** KaiC$_{RS}$-S413E/S414E:KaiB$_{RS}$ complex. To validate the final combined dodecamer structures, the data were reprocessed for the full dodecamer. The figure shows representative good class averages, the final reconstruction, angular distribution and Fourier shell correlation curve for the **(c)** KaiC$_{RS}$-S413E/S414E alone and **(d)** KaiC$_{RS}$-S413E/S414E:KaiB$_{RS}$ complex dodecamers. **(e)** Comparison of the C1 and D6 reconstructions of KaiC$_{RS}$-S413E/S414E alone and KaiC$_{RS}$-S413E/S414E:KaiB$_{RS}$, and Fourier shell correlation curves for the C1 reconstructions. The C1/D6 comparisons do not reveal discernable differences, suggesting that these complexes have D6 symmetry.

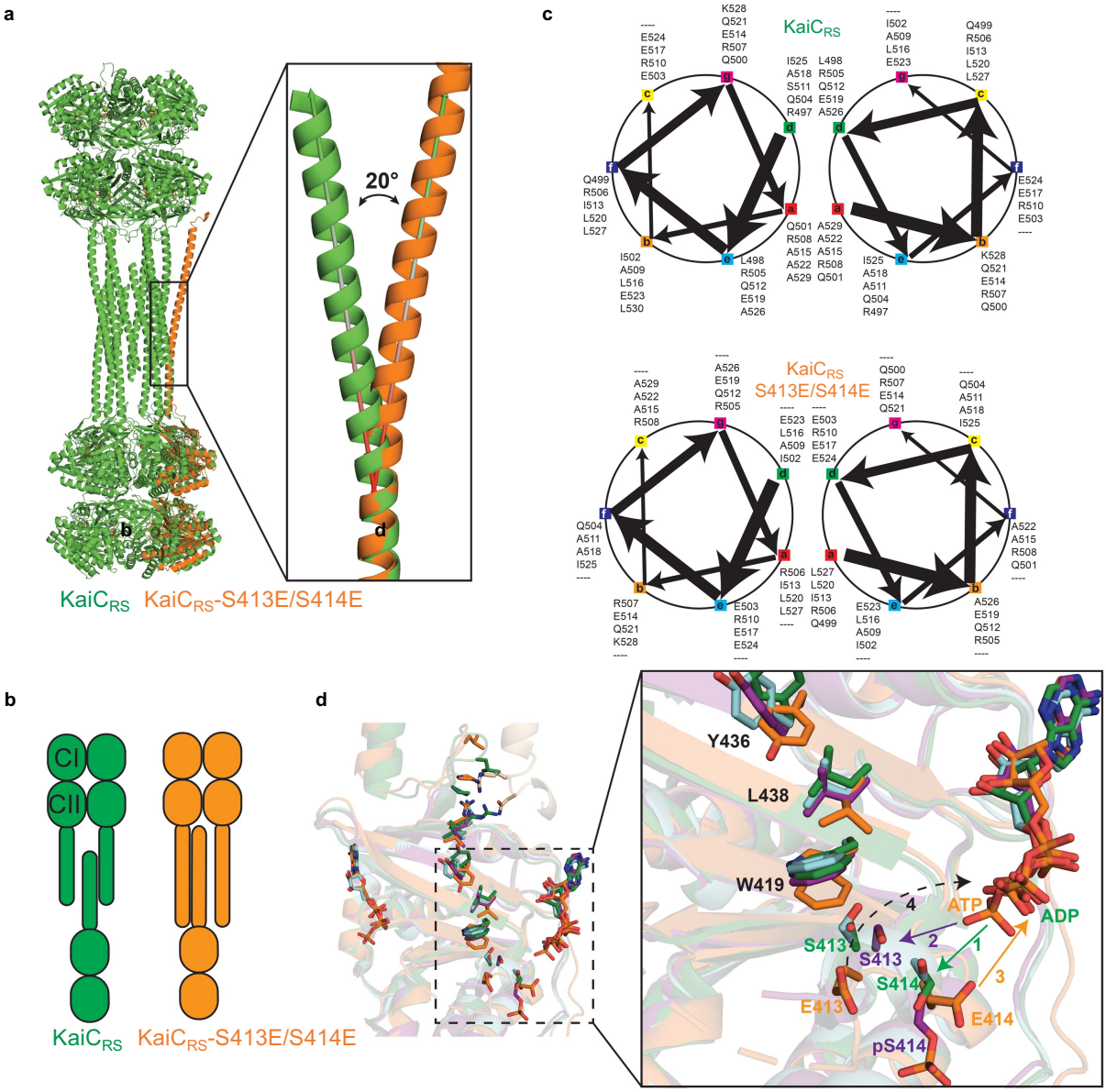

Extended Data Fig. 5 | Correlation between the coiled-coil register shift and phosphorylation, and model for consecutive phosphorylation/dephosphorylation events in CII domain of KaiC$_{RS}$. (a) Structural comparison between KaiC$_{RS}$ (green) and KaiC$_{RS}$-S413E/S414E (orange, single chain for clarity) reveals that the coiled-coil in the phosphomimetic structure points outwards, with an angle of about 20° relative to the KaiC$_{RS}$ coiled-coil. **(b)** The conformational change in the coiled-coil domain affects the dimer interface due to partner swaps with the opposite hexamer (see also Fig. 2). From an "outside perspective": the C-terminal helix in KaiC$_{RS}$ interacts with the right chain from the opposite hexamer, whereas in KaiC$_{RS}$-S413E/S414E the interaction is with the chain on the left. **(c)** Coiled-coil diagrams describe the heptad register shift that accompanies this structural rearrangement. **(d)** Based on the overlay of our structures, we propose the following model for the phosphorylation/dephosphorylation events. First, the phosphorylation cycle starts with the transfer of the γ-phosphate of ATP to the hydroxyl group of Ser^{414} (1; green arrow) in unphosphorylated KaiC$_{RS}$ (green) or KaiC$_{RS}$-Δcoil (cyan). Secondly, pSer^{414} of KaiC$_{RS}$-Δcoil (purple, singly phosphorylated) moves away from the active site placing the hydroxyl group of Ser^{413} closer to the γ-phosphate of ATP for the second phosphorylation (2; purple arrow). Thirdly, the doubly phosphomimetic state (KaiC$_{RS}$-S413E/S414E, orange) reveals that the phosphoryl group of pSer^{414} moves back towards the active site for dephosphorylation (3; orange arrow). Lastly, we hypothesize that the indole group of Trp^{419} "pushes" pSer^{413} into the active site for the second dephosphorylation event (dashed arrow), in agreement with the slower dephosphorylation rate observed in the KaiC$_{RS}$-Δcoil construct (*cf.* Fig. 2d).

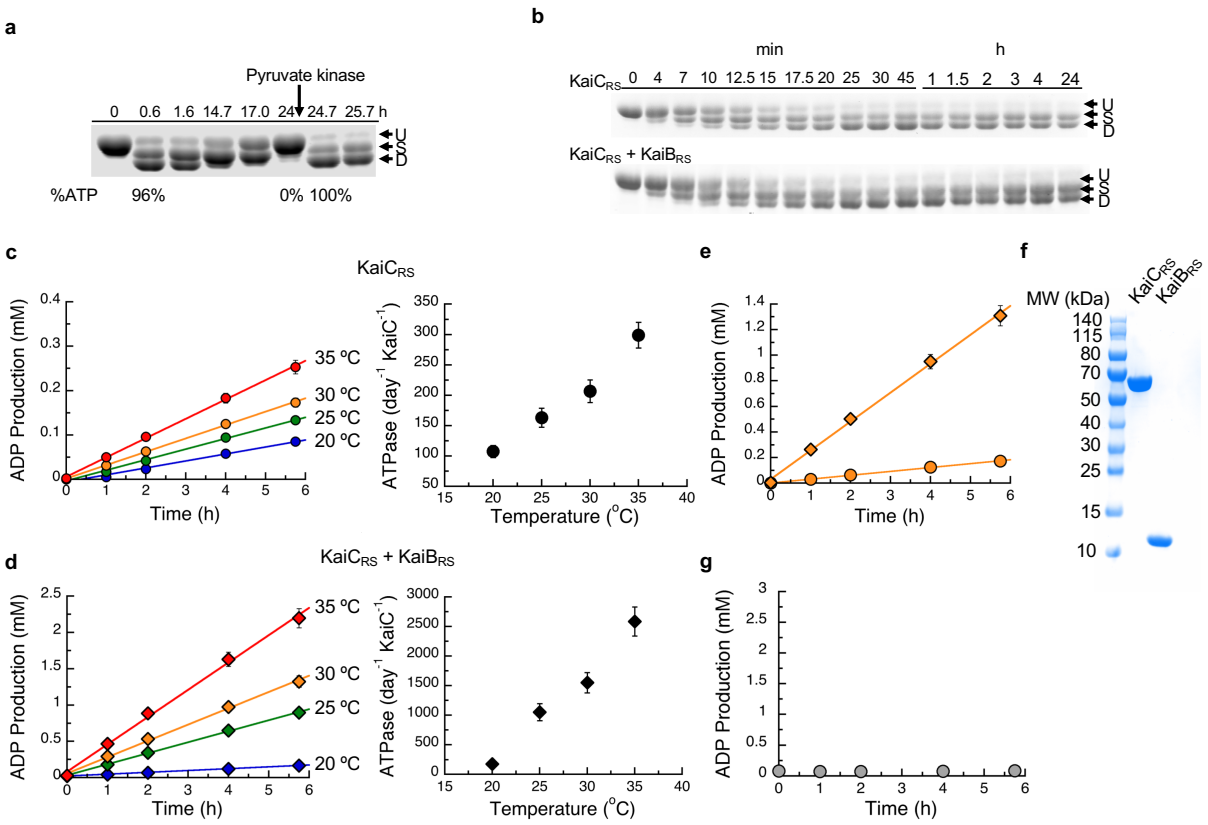

Extended Data Fig. 6 | Effect of ATP-to-ADP ratio on $KaiC_{RS}$ auto-dephosphorylation and the dependence of temperature and $KaiB_{RS}$ binding on the ATPase activity of $KaiC_{RS}$. **(a)** 10% SDS-PAGE gel of 3.5 μM KaiCRS and 3.5 μM KaiBRS in the presence of 4 mM ATP and 10 mM phosphoenolpyruvate at 30 °C shows that the auto-phosphorylation cycle restarts upon regeneration of ATP by the addition of 2 U/mL pyruvate kinase at the 24-hour time mark. **(b)** 10% SDS-PAGE gel of 3.5 μM $KaiC_{RS}$ without (upper panel) and with (lower panel) 3.5 μM $KaiB_{RS}$ in the presence of 4 mM ATP with an ATP-recycling system added from the beginning showing that under these conditions KaiB does not accelerate dephosphorylation. **(c)** Representative curves for ADP production of $KaiC_{RS}$ (3.5 μM) alone and **(d)** in the presence of $KaiB_{RS}$ (3.5 μM) in 4 mM ATP measured by HPLC. The data were analyzed as described in the Methods section and result in ATPase activities of 108 ± 10 day^{-1} KaiC^{-1} (with $KaiB_{RS}$ = 176 ± 29 day^{-1} KaiC^{-1}) at 20 °C, 163 ± 16 day^{-1} KaiC^{-1} (with $KaiB_{RS}$ = 1052 ± 143 day^{-1} KaiC^{-1}) at 25 °C, 208 ± 19 day^{-1} KaiC^{-1} (with $KaiB_{RS}$ = 1557 ± 172 day^{-1} KaiC^{-1}) at 30 °C, and 300 ± 21 day^{-1} KaiC^{-1} (with $KaiB_{RS}$ = 2584 ± 245 day^{-1} KaiC^{-1}) at 35 °C. The temperature coefficient, Q_{10}, was calculated using the data obtained at 25 °C and 35 °C and yields a value of ~ 1.9. The standard deviations of ATPase activity at each temperature were obtained from three replicate measurements. **(e)** The comparison of ADP production of $KaiC_{RS}$ in the absence (orange circles) and presence (orange diamonds) of $KaiB_{RS}$ at 30 °C indicate a 7.5-fold increase in ATPase activity for the complex. The binding of $KaiB_{RS}$ accelerates the ATPase activity of $KaiC_{RS}$ in both the CI and CII domains (see also Extended Data Fig. 8b, c). **(f)** The SDS-PAGE gel of $KaiC_{RS}$ (10 μg) and $KaiB_{RS}$ (10 μg) shows that both proteins were purified to homogeneity and the measured ATPase activity is, therefore, not due to impurities. **(g)** ADP production of $KaiB_{RS}$ in 4 mM ATP at 30 °C shows, as expected, no ATPase activity for $KaiB_{RS}$ alone and confirms the increase in ATPase activity shown in panel (d) is due to complex formation.

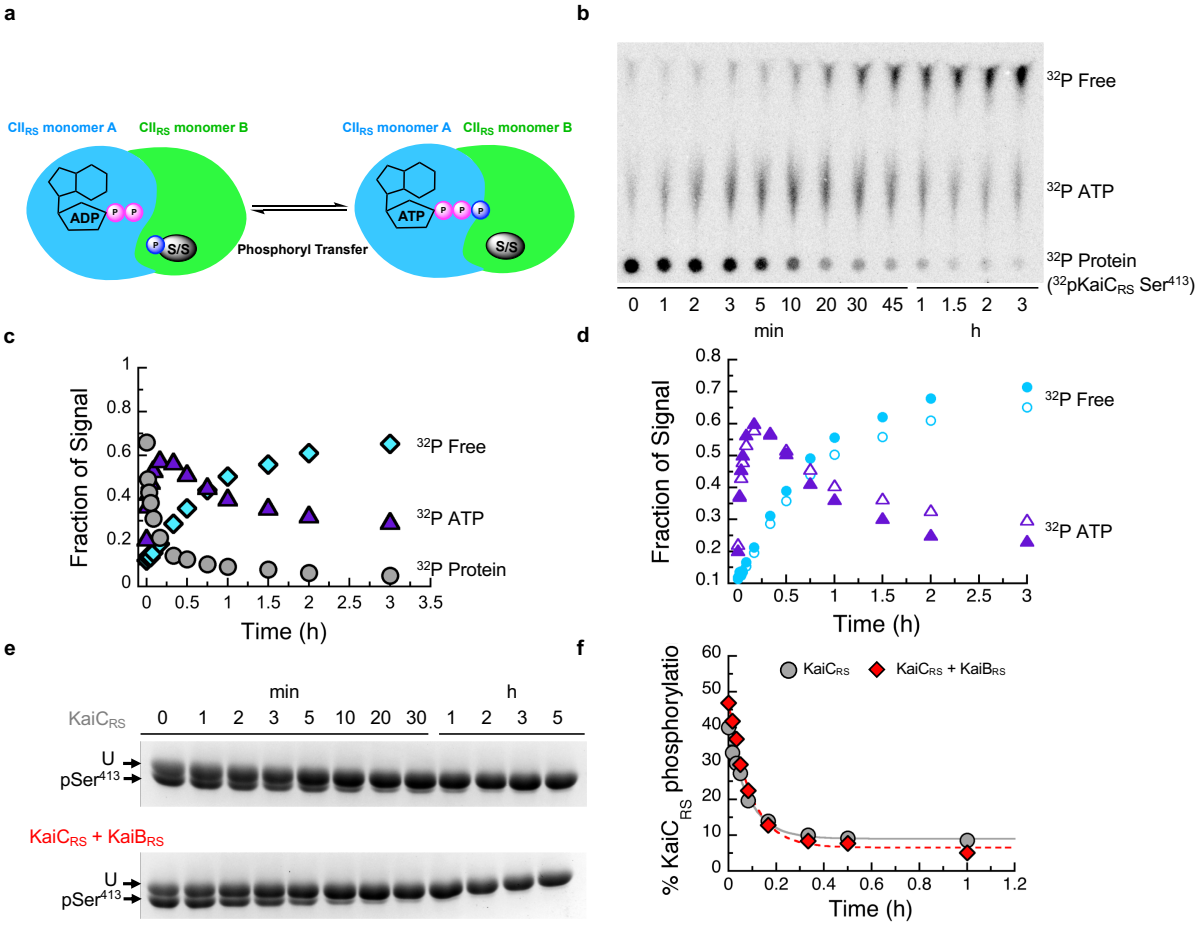

Extended Data Fig. 7 | Dephosphorylation of $KaiC_{RS}$ occurs via an ATP-synthase mechanism and the phosphoryl-transfer step is unaffected by the binding of $KaiB_{RS}$. (a) Possible mechanisms how $KaiB_{RS}$ could accelerate $KaiC_{RS}$ dephosphorylation at nighttime. Binding of $KaiB_{RS}$ on the CII_{RS} domain directly accelerates the phosphoryl transfer from pSer to bound ADP to generate transiently bound ATP. The cartoon represents the interface between two monomers in the CII_{RS} domain. **(b)** Autoradiograph of separation of ^{32}P-$KaiC_{RS}$ at Ser^{413}, transiently formed ^{32}P-ATP, and free ^{32}Pi via thin-layer chromatography (TLC) with 4 mM ADP at 30 °C, with the corresponding kinetics shown in **(c)** where gray circle, purple triangle, and cyan diamonds represent the relative concentrations of phosphorylated ^{32}P-$KaiC_{RS}$, ^{32}P-ATP, and free ^{32}Pi, respectively. **(d)** Comparison of transient ^{32}P-ATP formation and decay in the absence (open triangle) and presence (solid triangle) of $KaiB_{RS}$ and free ^{32}P formation in the absence (open circles) and presence of $KaiB_{RS}$ (solid circles). Faster decay of transient ^{32}P-ATP together with higher free ^{32}P production in the presence of $KaiB_{RS}$ indicated that $KaiB_{RS}$ accelerates hydrolysis in $KaiC_{RS}$. **(e)** SDS-PAGE gel (10%) of dephosphorylation of phosphorylated 3.5 μM $KaiC_{RS}$ at Ser^{413} without (upper gel) and with (lower gel) 3.5 μM $KaiB_{RS}$ in the presence of 4 mM ADP at 30 °C. **(f)** Densitometric analysis of data in panel (e) shows the decay of total $KaiC_{RS}$ phosphorylation in the absence (gray circles) and presence (red diamonds) of $KaiB_{RS}$ and yields rates of 11.5 ± 0.8 h^{-1} and 11.0 ± 0.8 h^{-1}, respectively. This result indicates that binding of $KaiB_{RS}$ does not accelerate the phosphoryl-transfer step in $KaiC_{RS}$.

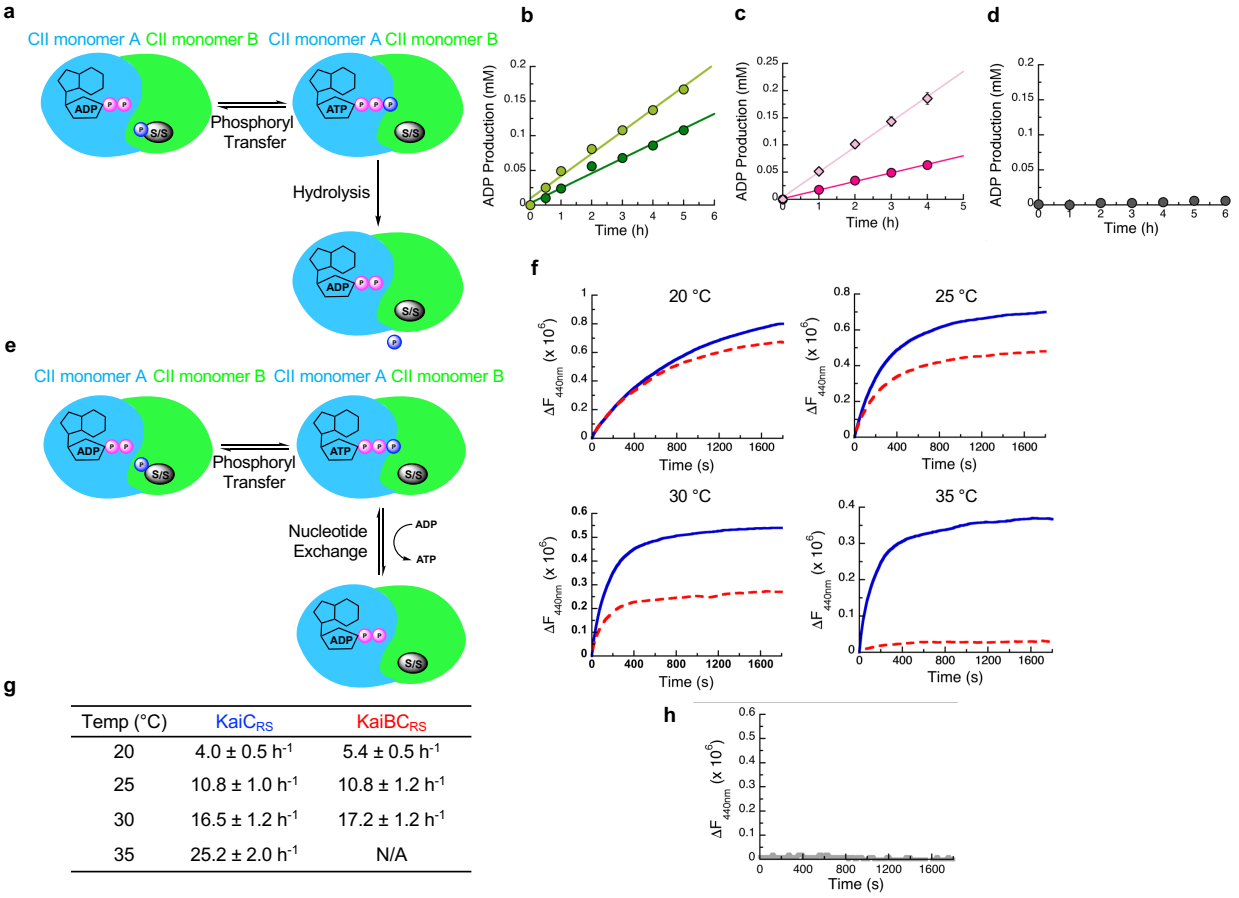

g

Temp (°C)	$KaiC_{RS}$	$KaiBC_{RS}$
20	4.0 ± 0.5 h^{-1}	5.4 ± 0.5 h^{-1}
25	10.8 ± 1.0 h^{-1}	10.8 ± 1.2 h^{-1}
30	16.5 ± 1.2 h^{-1}	17.2 ± 1.2 h^{-1}
35	25.2 ± 2.0 h^{-1}	N/A

Extended Data Fig. 8 | Effect of $KaiB_{RS}$ binding on ATPase activity and nucleotide exchange in the CII domain of $KaiC_{RS}$. **(a)** Second possible mechanism to explain how $KaiB_{RS}$ accelerates $KaiC_{RS}$ dephosphorylation at nighttime: binding of $KaiB_{RS}$ to the CI_{RS} domain could increase the hydrolysis rate in the CII_{RS} domain and, thereby, prevent the phosphoryl transfer back from transiently formed or external ATP back to serine residues. **(b)** ADP production of phosphorylated $KaiC_{RS}$ with catalytic mutations in the CI domain ($KaiC_{RS}$-E62Q/E63Q, 3.5 μM) in the absence (dark green circles) and presence (light green circles) of 3.5 μM $KaiB_{RS}$ at 30 °C with 4 mM ATP was quantified using HPLC. From these data an ATPase activity in the CII domain of 112 ± 8 day^{-1} $KaiC^{-1}$ and 195 ± 16 day^{-1} $KaiC^{-1}$ in the presence of $KaiB_{RS}$ was determined. **(c)** ADP production measured by HPLC as in panel (b) of $KaiC_{RS}$ but with catalytic mutations in the CII domain ($KaiC_{RS}$-E302Q/E303Q, 3.5 μM) in the absence (dark pink circles) and presence (light pink diamonds) of 3.5 μM $KaiB_{RS}$. The corresponding ATPase activities in the CI domain are 110 ± 12 day^{-1} $KaiC^{-1}$ in the absence and 320 ± 22 day^{-1} $KaiC^{-1}$ in the presence of $KaiB_{RS}$. **(d)** ADP production of $KaiCI_{RS}$-E62Q/E63Q (construct of only CI domain with catalytic mutations) in 4 mM ATP at 30 °C shows no ATPase activity indicating that Glu^{62} and Glu^{63} are the only two residues that are responsible for ATPase activity in CI domain of $KaiC_{RS}$ and confirms the ATPase activity shown in panel C is due to ATPase activity in CII domain of $KaiC_{RS}$. **(e)** Third possible mechanism to explain how $KaiB_{RS}$ accelerates $KaiC_{RS}$ dephosphorylation at nighttime: binding of $KaiB_{RS}$ to the CI_{RS} domain could promote faster nucleotide exchange in the CII_{RS} domain to displace transient ATP by ADP. **(f)** Time course of fluorescence intensity at 440 nm due to binding of mant-ATP to $KaiC_{RS}$-S413E bound with ATP in the absence (solid blue trace) and presence (red dotted trace) of $KaiB_{RS}$. $KaiC_{RS}$-S413E (3.5 μM) was pre-incubated with 3.5 μM $KaiB_{RS}$ for 16 h at 20, 25, 30, and 35 °C in the presence of 50 μM ATP and an ATP-recycling system and then mixed with 250 μM mant-ATP. The observed exchange rates at each temperature are listed in the table **(g)**. **(h)** Nucleotide exchange of $KaiCI_{RS}$ (i.e., only CI_{RS} domain) cannot be measured since there is no tryptophan residue in close proximity of the nucleotide binding site. In summary, $KaiB_{RS}$ accelerates $KaiC_{RS}$ dephosphorylation by increasing the hydrolysis rate in the CI and CII domains and does not affect the nucleotide exchange rate. Representative traces are shown in (f) and (h) and the fitted parameters (g; mean ± S.D) were obtained from three replicate measurements.

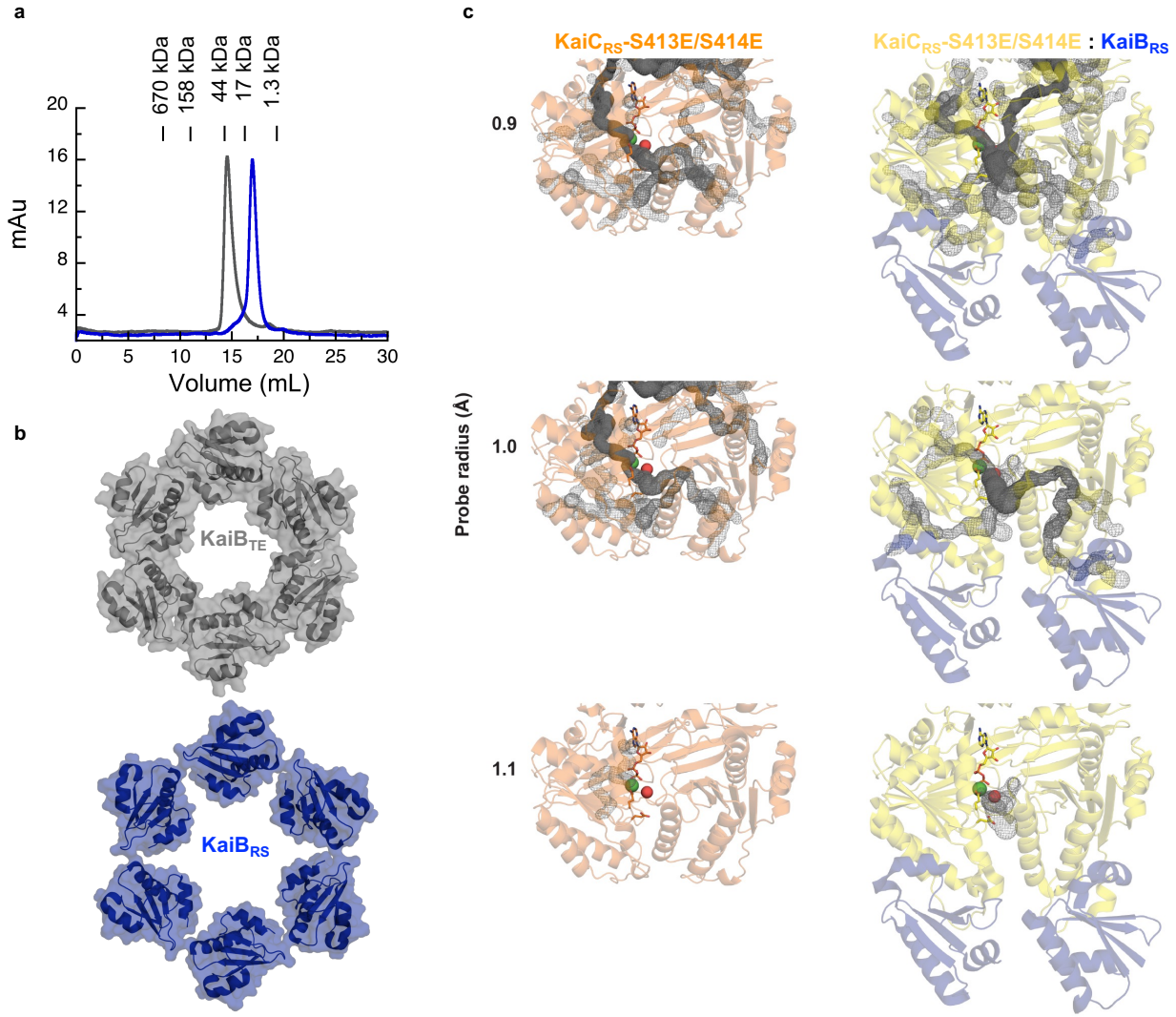

Extended Data Fig. 9 | KaiB-KaiB interface in the KaiBC$_{RS}$ complex affects the solvent accessibility into the active site of KaiC$_{RS}$-CI (**a**) Size-exclusion chromatography of KaiB$_{RS}$ (blue) shows that it is monomeric in solution in contrast to KaiB$_{SE}$ (gray), which elutes as a tetramer. Molecular-weight standards are shown above the chromatogram. **(b)** Structural comparison of KaiB$_{TE}$ (gray, PDB 5jwq[26]) and KaiB$_{RS}$ (blue) when bound to their corresponding KaiC hexamers. The PISA software package[37] determines that for the KaiBC$_{TE}$ complex the interface between the KaiB$_{TE}$ monomers is 255 Å^2, whereas the average interface between KaiB$_{RS}$ monomers is only 45 Å^2 in the KaiBC$_{RS}$ complex. **(c)** To understand how KaiB$_{RS}$ binding to KaiC$_{RS}$-CI domain increases the hydrolysis rate, we investigated whether conformational changes modulated substrate access to the active site. The CAVER software[39] was used to calculate tunnels (gray mesh) leading into the active site of the CI domain of KaiC$_{RS}$-S413E/S414E alone (orange) and the KaiC$_{RS}$-S413E/S414E:KaiB$_{RS}$ complex (yellow:blue) with varying probe radii. In both structures, the active site was occupied by ADP:Mg^{2+} (sticks and green sphere, respectively). The crystal structure of bovine F1-ATPase in complex with a transition-state analogue (PDB 1w0j, chain D)[40] was used as a reference to determine the position of the catalytic water molecule in the active site (shown as a red sphere). The calculated tunnels connect bulk solvent to the catalytic water when KaiB$_{RS}$ is bound for probe radii larger than the default value of 0.9 Å, but never in its absence. These results suggest that KaiB$_{RS}$ facilitates the access of water into the active site of KaiC$_{RS}$-CI via long-range conformational changes and thus enhances ATP hydrolysis.

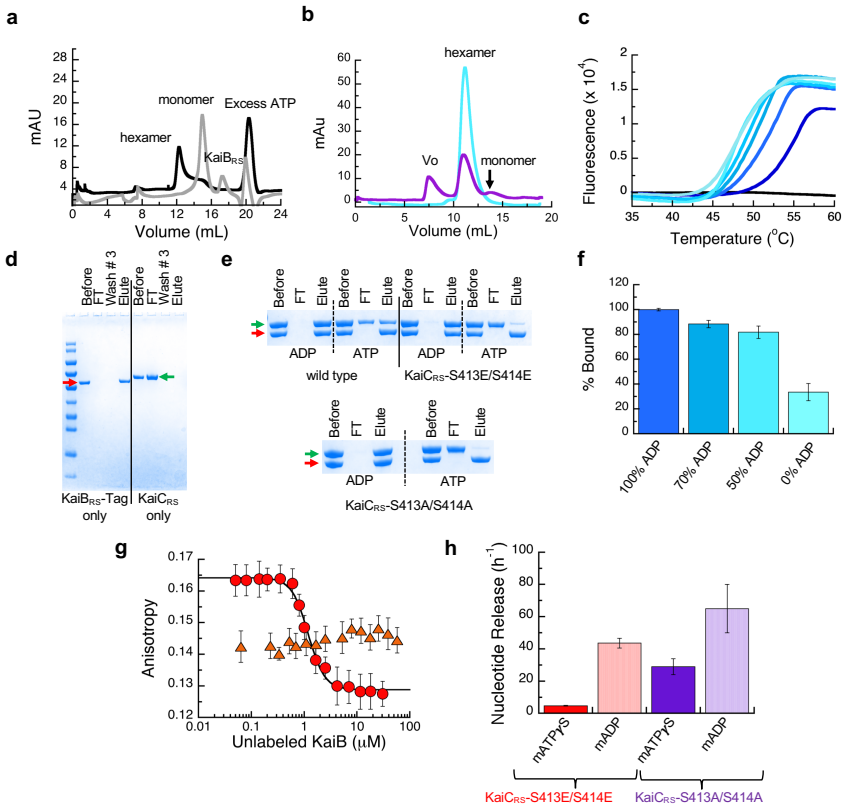

Extended Data Fig. 10 | $KaiB_{RS}$ binds preferentially to the post-hydrolysis state of $KaiC_{RS}$ and affects its stability. (a) Size-exclusion chromatography of 50 μM $KaiC_{RS}$-CI (CI domain) in the absence (black line, hexamer) and presence (gray line, monomer) of 50 μM $KaiB_{RS}$ in 1 mM ATP buffer. **(b)** Size-exclusion chromatography of 50 μM $KaiC_{RS}$-Δcoil in the presence of 50 μM $KaiB_{RS}$ (purple). The reference sample (50 μM $KaiC_{RS}$-Δcoil) is a hexamer in solution (cyan) and after the addition of 50 μM $KaiB_{RS}$ the mixture was incubated at 30 °C for 3.5 h (purple) before running the samples again on a Superdex-200 10/300 GL column at 4 °C. These data show that binding of $KaiB_{RS}$ results in (i) disassembly of the hexameric $KaiC_{RS}$-Δcoil structure into its monomers and (ii) aggregation as detected by the elution in the void volume of the column (v_0). **(c)** Thermal denaturation profiles for $KaiC_{RS}$-S413E/S414E in the presence of 1 mM ADP are shown from dark to light blue for increasing concentrations of $KaiB_{RS}$ (between 0 – 4 μM). The black line represents $KaiB_{RS}$ alone (15 μM), which shows no fluorescence signal as it does not bind to SYPRO Orange due to a lack of a hydrophobic core. The T_m decreases upon the addition of $KaiB_{RS}$, indicating that binding of $KaiB_{RS}$ destabilizes the $KaiC_{RS}$ dodecamer. Likely due to loosening up of interface and the $KaiC_{RS}$ structure, thereby allowing for the formation of a tunnel that connects bulk solvent to the position of the hydrolytic water in the active site (see Extended Data Fig. 9). **(d)** SDS-PAGE analysis showing the control experiment for pull-down assay. The first four lanes after the molecular weight marker are $KaiB_{RS}$-Tag samples (red arrow) and show that $KaiB_{RS}$-Tag binds tightly to the column. The last four lanes are control pull-down assay experiments for $KaiC_{RS}$ (green arrow) and show that $KaiC_{RS}$ alone is unable to bind to the column. The lanes represent the initial sample used in pull-down assay (Before), flow-through after loading sample onto the column (FT), flow-through after washing the column three times with the binding buffer (Wash #3), and sample after elution with imidazole (Elute). **(e)** SDS-PAGE analysis of pull-down assay to measure the complex formation between $KaiB_{RS}$-Tag and wild-type $KaiC_{RS}$, $KaiC_{RS}$-S413E/S414E, or $KaiC_{RS}$-S413A/S414A in the presence of 4 mM ADP or ATP (with an ATP-recycling system). **(f)** Percentage of wild-type $KaiC_{RS}$ bound to $KaiB_{RS}$-Tag protein for different ATP-to-ADP ratios (4 mM total nucleotide concentration) at 25 °C as measured from pull-down assays. **(g)** Fluorescence anisotropy at 30 °C of unlabeled $KaiB_{RS}$ competitively replacing the fluorophore-labeled $KaiB_{RS}$ ($KaiB_{RS}$-6IAF) from $KaiC_{RS}$-S413E/S414E in the presence of 4 mM ADP (red circles, K_D value of 0.79 ± 0.06 μM) and 4 mM ATP with an ATP-recycling system (orange triangles). In the latter experiment no change in anisotropy is observed, indicating that only a small fraction of $KaiB_{RS}$-6IAF is bound under these conditions. The average anisotropy and standard error were calculated from ten replicate measurements. **(h)** The mant-ATPγS or mant-ADP release is shown as bar graphs with observed rates of 4.8 ± 0.2 h^{-1} and 43.6 ± 3.0 h^{-1} for mant-ATPγS and mant-ADP releasing from $KaiC_{RS}$-S413E/S414E, respectively, and 21.0 ± 3.0 h^{-1} and 65 ± 15 h^{-1} for mant-ATPγS and mant-ADP releasing from $KaiC_{RS}$-S413A/S414A, respectively. The result shows that CII domain of $KaiC_{RS}$ prefers binding of ATP over ADP. Experiments in panels f and h were performed in triplicate with error bars representing SD.

Extended Data Table 1 | X-ray crystallography data collection and refinement statistics

	$KaiC_{RS}$ PDB: 8dba (oligomeric state: dodecamer)	$KaiC_{RS}$-Δcoil PDB: 8db3 (oligomeric state: hexamer)
Data collection		
Space group	P1	$C222_1$
Cell dimensions		
a, *b*, *c* (Å)	105.11, 136.09, 146.2	94.06, 197.28, 150.19
α, β, γ (°)	93.13, 94.43, 108.09	90, 90, 90,
Resolution (Å)	47.65 - 3.5 (3.625 - 3.5)*	53.89 - 2.9 (3.004 - 2.9)*
R_{sym} or R_{merge}	0.2213 (1.372)	0.4267 (2.994)
$I / \sigma I$	2.57 (0.73)	5.54 (1.15)
Completeness (%)	97.62 (94.08)	99.89 (99.97)
Redundancy	1.9 (2.0)	7.2 (7.3)
Refinement		
Resolution (Å)	3.5	2.9
No. reflections	94151 (9047)	31344 (3102)
R_{work} / R_{free}	0.2323/ 0.2775	0.2308/0.2892
No. atoms	47510	10293
Protein	46772	10131
Ligand/ion	948	231
Water	67	0
B-factors		
Protein	102.48	56.06
Ligand/ion	89.08	44.62
Water	72.52	-
R.m.s. deviations		
Bond lengths (Å)	0.002	0.004
Bond angles (°)	0.62	0.73

*Values in parentheses are for highest-resolution shell.
A single crystal was used for each structure.

Extended Data Table 2 | Cryo-EM data collection, refinement, and validation statistics

	$KaiC_{RS}$-S413E/S414E (EMDB-xxxx) (PDB xxxx) (oligomeric state: dodecamer)	$KaiC_{RS}$-S413E/S414E:$KaiB_{RS}$ (EMDB-xxxx) (PDB xxxx) (oligomeric state: dodecamer)
Data collection and processing		
Magnification		
Voltage (kV)	300	300
Electron exposure (e–/Å^2)	91.7	94.5
Defocus range (μm)		
Pixel size (Å)	1.074	1.023
Symmetry imposed	C6	C6
Initial particle images (no.)	82,500	440,00
Final particle images (no.)	32,000	190,000
Map resolution (Å)	2.9	2.6
FSC threshold	0.143	0.143
Map resolution range (Å)		
Refinement		
Initial model used (PDB code)	$KaiC_{RS}$ (this study)	$KaiC_{RS}$ (this study), 5jwo[26]
Model resolution (Å)	3.0	3.1
FSC threshold	0.143	0.143
Model resolution range (Å)		
Map sharpening *B* factor (Å^2)		
Model composition		
Non-hydrogen atoms	51,828	59,520
Protein residues	6,576	7,644
Ligands	48	48
B factors (Å^2)		
Protein	51.86	63.16
Ligand	42.31	76.06
R.m.s. deviations		
Bond lengths (Å)	0.003	0.009
Bond angles (°)	0.677	0.931
Validation		
MolProbity score	2.22	2.84
Clashscore	17.99	25.00
Poor rotamers (%)	2.30	3.61
Ramachandran plot		
Favored (%)	96.88	90.81
Allowed (%)	2.94	9.19
Disallowed (%)	0.18	0.00

Extended Data Table 3 | Codon-optimized DNA sequence for $KaiC_{RS}$ and $KaiB_{RS}$ constructs

Protein	Plasmid	DNA Sequence
$KaiC_{RS}$	pETM-41	ATGGGCATCGGCAAGAGCCCGACCGGCATTCAGGGTTTCGACGAACTGACCCTGGGT GGCCTGCCGACCGGCCGTCCGAGCCTGGTTTGCGGTAGCGCGGGTTGCGGTAAAACC CTGTTCGCGAGCACCTTTCTGATTAACGGCGTGCGTGATCACGGCGAACCGGGTGTT TTCGTGACCTTTGAGGAACGTCCGGAGGACATCGTTAACAACGTGGCGAGCCTGGGT TTCGAACTGGATAAGCTGATCGAGGAAGAGAAAATCGCGATTGAGCACATTGCGGTT GACCCGAGCGAAGTGGCGGAGATCGGCGACTACGATCTGGAGGGTCTGTTTCTGCGT CTGGAACTGGCGATTGACACCGTTGGTGCGAAGCGTGTGGTTCTGGATACCATCGAA AGCCTGTTCAGCGCGTTTAGCAACCCGGCGATCCTGCGTGCGGAGATTCGTCGTCTG TTCGACTGGCTGAAAGAACGTGGCCTGACCACCGTGATTACCGCGGAGCGTGGCGAT GGTGCGCTGACCCGTCAAGGTCTGGAAGAGTATGTTAGCGACTGCGTGATCCTGCTG GATCACCGTGTTGAGAACCAGATCAGCACCCGTCGTCTGCGTATTGTGAAGTACCGT GGCACCGCGCACGGCACCAACGAATATCCGTTCCTGATCGACACCGATGGCTTTAGC GTTCTGCCGGTGAGCGCGCTGGGTCTGCTGCACCAAGTTCACGAAGAGCGTATTGCG AGCGGTGTGCCGGACCTGGATGCGATGATGGCGGGTGGCGGTTTCTTTCGTGGCAGC AGCATTCTGGTTAGCGGTGTGGCGGGTGCGGGTAAAAGCAGCCTGGCGGCGCACTTT GCTGCGGCGGCGTGCGCGCGTGGCGAGCGTGCGATGTACTTCAGCTTTGAAGAGGCG GCGGATCAGGCGGTTCGTAACATGCGTAGCCTGGGCCTGGACCTGGGTCGTTGGCGT GATGCGGGTCTGCTGCGTTTCATGGCGACCCGTCCGACCTTTTATAGCCTGGAAATG CACCTGGCGGTTATTCTGCGTGAGGTGATGCGTTTCGAACCGAGCGTGGTTGTGCTG GACCCGATCAGCGCGTTTACCGAGAGCGGTGATCGTCTGGAAGTTCAAAGCATGCTG CTGCGTATTGTGGACTTCCTGAAGAACCGTGGCATCACCGGTATTTTTACCCACCTG GCGCACAGCCAAAACGAGGCGACCACCGATGCGGGCCTGAGCAGCCTGATGGATGGT TGGGTTCTGATGCTGAACCGTGAAGTGAACGGCGAGTTCAACCGTGAACTGTACCTG CTGAAGGCGCGTGGTATGGCGCACAGCAACCAAGTTCGTGAGTTTCTGATGAGCGAT CGTGGTATTAGCCTGCTGCCGCCGCACCTGGGTGAAGGCGGTGCGCTGACCGGCACC GCGCGTAAAGCGGAAGAGGCGCGTCTGCGTCGTGCGGAAATCGAGCGTCAGACCGAG CTGGGTCGTCTGCAGCAACAGATTGAACAACGTCGTCGTCGTGCGCGTGCGCAGATT GAGGCGCTGGAAGCGGAGCTGCAAGCGGAAGAGATCGCGCTGAAGGCGCTGGTTGAG AGCGAGAGCGCGCATGAACGTCAACGTCTGGCGGATGCGGATACCCTGGCGCGTAGC CGTGGCAACGAACGTTTCGCGGACCTGCTGATGAACAAAGGTGAG
$KaiB_{RS}$	pETM-41	ATGGGTCGTCGTCTGGTGCTGTATGTGGCGGGTCAAACCCCGAAAAGCCTGGCGGCG ATTAGCAACCTGCGTCGTATCTGCGAGGAAAACCTGCCGGGCCAGTACGAGGTGGAA GTTATCGACCTGAAGCAAAACCCGCGTCTGGCGAAAGAGCACAGCATCGTGGCGATT CCGACCCTGGTGCGTGAACTGCCGGTTCCGATCCGTAAGATTATTGGTGACCTGAGC GATAAAGAACAAGTGCTGGTGAACCTGAAAATGGACATGGAG
		Protein Sequence
$KaiC_{RS}$	pETM-41	*GAMGIGKSPTGIQGFDELTLGGLPTGRPSLVCGSAGCGKTLFASTFLINGVRDHGEP GVFVTFEERPEDIVNNVASLGFELDKLIEEEKIAIEHIAVDPSEVAEIGDYDLEGLF LRLELAIDTVGAKRVVLDTIESLFSAFSNPAILRAEIRRLFDWLKERGLTTVITAER GDGALTRQGLEEYVSDCVILLDHRVENQISTRRLRIVKYRGTAHGTNEYPFLIDTDG FSVLPVSALGLLHQVHEERIASGVPDLDAMMAGGGFFRGSSILVSGVAGAGKSSLAA HFAAAACARGERAMYFSFEEAADQAVRNMRSLGLDLGRWRDAGLLRFMATRPTFYSL EMHLAVILREVMRFEPSVVVLDPISAFTESGDRLEVQSMLLRIVDFLKNRGITGIFT HLAHSQNEATTDAGLSSLMDGWVLMLNREVNGEFNRELYLLKARGMAHSNQVREFLM SDRGISLLPPHLGEGGALTGTARKAEEARLRRAEIERQTELGRLQQQIEQRRRRARA QIEALEAELQAEEIALKALVESESAHERQRLADADTLARSRGNERFADLLMNKGE
$KaiB_{RS}$	pETM-41	*GAMGRRLVLYVAGQTPKSLAAISNLRRICEENLPGQYEVEVIDLKQNPRLAKEHSIV AIPTLVRELPVPIRKIIGDLSDKEQVLVNLKMDME

*GA are residues that are part of the after TEV protease recognition site and remain after cleavage. Residue numbering of both $KaiC_{RS}$ and $KaiB_{RS}$ start counting after residues GA.

Extended Data Table 4 | Primers for site-directed mutagenesis and sequencing of $KaiC_{RS}$

Mutation		Primer
$KaiC_{RS}$ S413E	5' GCGACCACCGATGCGGGCCTGGAAAGCCTGATGGATGGTTGGGTTC 3'	Forward
	5' GAACCCAACCATCCATCAGGCTTTCCAGGCCCGCATCGGTGGTCGC 3'	Reverse
$KaiC_{RS}$ S413E/S414E	5' GCGACCACCGATGCGGGCCTGGAAGAACTGATGGATGGTTGGGTTC 3'	Forward
	5' GAACCCAACCATCCATCAGTTCTTCCAGGCCCGCATCGGTGGTCGC 3'	Reverse
$KaiC_{RS}$ S413A/S414A	5' GAGGCGACCACCGATGCGGGCCTGGCGGCGCTGATGGATGGTTGGGTTCTGATG 3'	Forward
	5' CATCAGAACCCAACCATCCATCAGCGCCGCCAGGCCCGCATCGGTGGTCGCCTC 3'	Reverse
$KaiC_{RS}$ E62Q/E63Q	5' CACGGCGAACCGGGTGTTTTCGTGACCTTTCAGCAACGTCCGGAGGACATCGTTAACAAC 3'	Forward
	5' GTTGTTAACGATGTCCTCCGGACGTTGCTGAAAGGTCACGAAAACACCCGGTTCGCCGTG 3'	Reverse
$KaiC_{RS}$ E302Q/E303Q	5' GTGCGATGTACTTCAGCTTTCAACAGGCGGCGGATCAGGC 3'	Forward
	5' GCCTGATCCGCCGCCTGTTGAAAGCTGAAGTACATCGCAC 3'	Reverse
$KaiC_{RS}$-ΔcoiI (residues 1–489)	5' GCGGAAGAGGCGCGTCTGCGTCGTGCGTAAATCGAGCGTCAGACCGAGCTGGGTCG 3'	Forward
	5' CGACCCAGCTCGGTCTGACGCTCGATTTACGCACGACGCAGACGCGCCTCTTCCGC 3'	Reverse
$KaiCI_{RS}$ (residues 1–230)	5' GACACCGATGGCTTTAGCGTTCTGTAGGTGAGCGCGCTGGGTCTGCTGCACCAA 3'	Forward
	5' TTGGTGCAGCAGACCCAGCGCGCTCACCTACAGAACGCTAAAGCCATCGGTGTC 3'	Reverse
*$KaiCI_{RS}$ E62Q/E63Q	5' CACGGCGAACCGGGTGTTTTCGTGACCTTTCAGCAACGTCCGGAGGACATCGTTAACAAC 3'	Forward
	5' GTTGTTAACGATGTCCTCCGGACGTTGCTGAAAGGTCACGAAAACACCCGGTTCGCCGTG 3'	Reverse

Reading area	Primer sequence
From MBP-Val^{260} to $KaiC_{RS}$-Gly^{160}	5' GGTGTAACGGTACTGCCGACC 3'
From Ala^{140} to Lys^{441}	5' GCGATTGACACCGTTGGT 3'
From Leu^{399} to Ser^{568}	5' AAGCATGCTGCTGCGTATTG 3'

*Using $KaiCI_{RS}$ as a template for site-directed mutagenesis

Reference

1 Ishiura, M. *et al.* Expression of a gene cluster kaiABC as a circadian feedback process in cyanobacteria. *Science* **281**, 1519-1523, doi:10.1126/science.281.5382.1519 (1998).

2 Cohen, S. E. & Golden, S. S. Circadian Rhythms in Cyanobacteria. *Microbiol Mol Biol Rev* **79**, 373-385, doi:10.1128/MMBR.00036-15 (2015).

3 Golden, S. S. Principles of rhythmicity emerging from cyanobacteria. *Eur J Neurosci* **51**, 13-18, doi:10.1111/ejn.14434 (2020).

4 Partch, C. L. Orchestration of Circadian Timing by Macromolecular Protein Assemblies. *J Mol Biol* **432**, 3426-3448, doi:10.1016/j.jmb.2019.12.046 (2020).

5 Rust, M. J., Markson, J. S., Lane, W. S., Fisher, D. S. & O'Shea, E. K. Ordered phosphorylation governs oscillation of a three-protein circadian clock. *Science* **318**, 809-812, doi:10.1126/science.1148596 (2007).

6 Dvornyk, V., Vinogradova, O. & Nevo, E. Origin and evolution of circadian clock genes in prokaryotes. *Proc Natl Acad Sci U S A* **100**, 2495-2500, doi:10.1073/pnas.0130099100 (2003).

7 Dvornyk, V. & Knudsen, B. Functional divergence of the circadian clock proteins in prokaryotes. *Genetica* **124**, 247-254, doi:10.1007/s10709-005-3146-0 (2005).

8 Holtzendorff, J. *et al.* Genome streamlining results in loss of robustness of the circadian clock in the marine cyanobacterium Prochlorococcus marinus PCC 9511. *J Biol Rhythms* **23**, 187-199, doi:10.1177/0748730408316040 (2008).

9 Axmann, I. M. *et al.* Biochemical evidence for a timing mechanism in prochlorococcus. *J Bacteriol* **191**, 5342-5347, doi:10.1128/JB.00419-09 (2009).

10 Ma, P., Mori, T., Zhao, C., Thiel, T. & Johnson, C. H. Evolution of KaiC-Dependent Timekeepers: A Proto-circadian Timing Mechanism Confers Adaptive Fitness in the Purple Bacterium Rhodopseudomonas palustris. *PLoS Genet* **12**, e1005922, doi:10.1371/journal.pgen.1005922 (2016).

11 Min, H., Guo, H. & Xiong, J. Rhythmic gene expression in a purple photosynthetic bacterium, Rhodobacter sphaeroides. *FEBS Lett* **579**, 808-812, doi:10.1016/j.febslet.2005.01.003 (2005).

12 Carter, A. P. *et al.* Structure and functional role of dynein's microtubule-binding domain. *Science* **322**, 1691-1695, doi:10.1126/science.1164424 (2008).

13 Schmelling, N. M. *et al.* Minimal tool set for a prokaryotic circadian clock. *BMC Evol Biol* **17**, 169, doi:10.1186/s12862-017-0999-7 (2017).

14 Aoki S, O. K. in *Bacterial circadian programs* (ed Mackey SR Ditty JL, Johnson CH) Ch. 15, 259 –282 (Springer, 2009).

15 Wiegard, A. *et al.* Biochemical analysis of three putative KaiC clock proteins from Synechocystis sp PCC 6803 suggests their functional divergence. *Microbiol-Sgm* **159**, 948-958, doi:10.1099/mic.0.065425-0 (2013).

16 Pattanayek, R. *et al.* Analysis of KaiA-KaiC protein interactions in the cyano-bacterial circadian clock using hybrid structural methods. *EMBO J* **25**, 2017-2028, doi:10.1038/sj.emboj.7601086 (2006).

17 Nishiwaki-Ohkawa, T., Kitayama, Y., Ochiai, E. & Kondo, T. Exchange of ADP with ATP in the CII ATPase domain promotes autophosphorylation of cyanobacterial clock protein KaiC. *Proc Natl Acad Sci U S A* **111**, 4455-4460, doi:10.1073/pnas.1319353111 (2014).

18 Kim, Y. I., Dong, G., Carruthers, C. W., Jr., Golden, S. S. & LiWang, A. The day/night switch in KaiC, a central oscillator component of the circadian clock of cyanobacteria. *Proc Natl Acad Sci U S A* **105**, 12825-12830, doi:10.1073/pnas.0800526105 (2008).
19 Swan, J. A. *et al.* Hidden conformations differentiate day and night in a circadian pacemaker. *bioRxiv*, 2021.2009.2014.460370, doi:10.1101/2021.09.14.460370 (2021).
20 Egli, M. *et al.* Loop-loop interactions regulate KaiA-stimulated KaiC phosphorylation in the cyanobacterial KaiABC circadian clock. *Biochemistry* **52**, 1208-1220, doi:10.1021/bi301691a (2013).
21 Hayashi, F. *et al.* ATP-induced hexameric ring structure of the cyanobacterial circadian clock protein KaiC. *Genes Cells* **8**, 287-296 (2003).
22 Nishiwaki, T. *et al.* Role of KaiC phosphorylation in the circadian clock system of Synechococcus elongatus PCC 7942. *Proc Natl Acad Sci U S A* **101**, 13927-13932, doi:10.1073/pnas.0403906101 (2004).
23 Xu, Y. *et al.* Identification of key phosphorylation sites in the circadian clock protein KaiC by crystallographic and mutagenetic analyses. *Proc Natl Acad Sci U S A* **101**, 13933-13938, doi:10.1073/pnas.0404768101 (2004).
24 Kitayama, Y., Iwasaki, H., Nishiwaki, T. & Kondo, T. KaiB functions as an attenuator of KaiC phosphorylation in the cyanobacterial circadian clock system. *EMBO J* **22**, 2127-2134, doi:10.1093/emboj/cdg212 (2003).
25 Chang, Y. G. *et al.* Circadian rhythms. A protein fold switch joins the circadian oscillator to clock output in cyanobacteria. *Science* **349**, 324-328, doi:10.1126/science.1260031 (2015).
26 Tseng, R. *et al.* Structural basis of the day-night transition in a bacterial circadian clock. *Science* **355**, 1174-1180, doi:10.1126/science.aag2516 (2017).
27 Abee, T., Hellingwerf, K. J. & Konings, W. N. Effects of potassium ions on proton motive force in Rhodobacter sphaeroides. *J Bacteriol* **170**, 5647-5653, doi:10.1128/jb.170.12.5647-5653.1988 (1988).
28 Terauchi, K. *et al.* ATPase activity of KaiC determines the basic timing for circadian clock of cyanobacteria. *Proc Natl Acad Sci U S A* **104**, 16377-16381, doi:10.1073/pnas.0706292104 (2007).
29 Nishiwaki, T. & Kondo, T. Circadian autodephosphorylation of cyanobacterial clock protein KaiC occurs via formation of ATP as intermediate. *J Biol Chem* **287**, 18030-18035, doi:10.1074/jbc.M112.350660 (2012).
30 Phong, C., Markson, J. S., Wilhoite, C. M. & Rust, M. J. Robust and tunable circadian rhythms from differentially sensitive catalytic domains. *Proc Natl Acad Sci U S A* **110**, 1124-1129, doi:10.1073/pnas.1212113110 (2013).
31 Murakami, R. *et al.* Cooperative Binding of KaiB to the KaiC Hexamer Ensures Accurate Circadian Clock Oscillation in Cyanobacteria. *Int J Mol Sci* **20**, doi:10.3390/ijms20184550 (2019).
32 Snijder, J. *et al.* Insight into cyanobacterial circadian timing from structural details of the KaiB-KaiC interaction. *Proc Natl Acad Sci U S A* **111**, 1379-1384, doi:10.1073/pnas.1314326111 (2014).
33 Rust, M. J., Golden, S. S. & O'Shea, E. K. Light-driven changes in energy metabolism directly entrain the cyanobacterial circadian oscillator. *Science* **331**, 220-223, doi:10.1126/science.1197243 (2011).

34 Truebestein, L. & Leonard, T. A. Coiled-coils: The long and short of it. *Bioessays* **38**, 903-916, doi:10.1002/bies.201600062 (2016).
35 Liu, J. & Rost, B. Comparing function and structure between entire proteomes. *Protein Sci* **10**, 1970-1979, doi:10.1110/ps.10101 (2001).
36 Pattanayek, R. *et al.* Visualizing a circadian clock protein: crystal structure of KaiC and functional insights. *Mol Cell* **15**, 375-388, doi:10.1016/j.molcel.2004.07.013 (2004).
37 Krissinel, E. & Henrick, K. Inference of macromolecular assemblies from crystalline state. *J Mol Biol* **372**, 774-797, doi:10.1016/j.jmb.2007.05.022 (2007).
38 Anisimova, M., Gil, M., Dufayard, J. F., Dessimoz, C. & Gascuel, O. Survey of branch support methods demonstrates accuracy, power, and robustness of fast likelihood-based approximation schemes. *Syst Biol* **60**, 685-699, doi:10.1093/sysbio/syr041 (2011).
39 Chovancova, E. *et al.* CAVER 3.0: a tool for the analysis of transport pathways in dynamic protein structures. *PLoS Comput Biol* **8**, e1002708, doi:10.1371/journal.pcbi.1002708 (2012).
40 Kagawa, R., Montgomery, M. G., Braig, K., Leslie, A. G. & Walker, J. E. The structure of bovine F1-ATPase inhibited by ADP and beryllium fluoride. *EMBO J* **23**, 2734-2744, doi:10.1038/sj.emboj.7600293 (2004).